Self-Assembly of Multinuclear Sandwich Silver(I) Complexes by Cooperation of Hexakis(azaheteroaryl)benzene Ligands, Argentophilic Interactions, and Fluoride Inclusion

Miha Drev, Uroš Grošelj, Drago Kočar, Franc Perdih, Jurij Svete, Bogdan Štefane, and Franc Požgan*

Faculty of Chemistry and Chemical Technology, University of Ljubljana, Večna pot 113, SI-1000 Ljubljana (Slovenia)

Table of Contents

Experimental Procedures

General information

All reagents were commercial-grade, and were used without further purification. Reactions were monitored by analytical thin-layer chromatography (TLC) on Fluka silica gel TLC. Merck silica gel 60 PF254 containing gypsum was used to prepare chromatotron plates. Radial chromatography was performed with a Harrison Research chromatotron, model 7924 T. Melting points were determined with SRS OptiMelt MPA100-Automated Melting Point System and are uncorrected. The NMR spectroscopy data were recorded at 296 K with Bruker Avance III 500 MHz for ^{1}H NMR, 126 MHz for ^{13}C NMR and 471 MHz for ^{19}F NMR. Variable temperature (240–330 K) ^{1}H NMR spectra were measured with Bruker DPX 300 MHz. Chemical shifts (in ppm) for ^{1}H NMR are referenced against TMS as an internal standard, or residual resonance of the protiated part of the deuterated solvent (2.05 ppm for acetone-d_6, and 1.94 ppm for CD_3CN). The ^{13}C NMR data are referenced against the central line of $CDCl_3$ (t, δ = 77.16 ppm) or acetone-d_6 (sept, 29.84 ppm). The coupling constants are given in Hertz (Hz). For the multiplicity signification, the standard abbreviation was used: s (singlet), d (doublet), t (triplet), q (quartet), sept (septet), and m (multiplet). IR spectra were obtained with a Bruker ALPHA FT-IR spectrophotometer and reported in reciprocal centimetres (cm^{-1}). High-resolution mass spectra were recorded with Agilent 6224 Accurate Mass TOF LC/MS and Thermo Fisher Q-Exactive instruments, while mass spectra were recorded with a Micromass Waters Q-Tof Premier instrument. Elemental analyses (C, H, N) were performed with a PerkinElmer 2400 Series II CHNS/O Analyzer. The reactions with microwave heating were performed with a CEM Discovery Microwave. The machine consists of a continuous, focused-microwave, power-delivery system with an operator-selectable power output from 0 to 300 W. Reactions were performed in glass vessels (capacity 10 mL) sealed with a septum. The pressure was controlled by a load cell connected to the vessel via the septum. The temperature of the content of the vessel was monitored using a calibrated, infrared, temperature controller mounted under the reaction vessel. All the mixtures were stirred with a Teflon-coated, magnetic stirring bar in the vessel. A ramp temperature of 5 min was set for each experiment.

Preparation of ligands 2 and 3

1,2,3,4,5,6-Hexa(pyridin-2-yl)benzene (2)

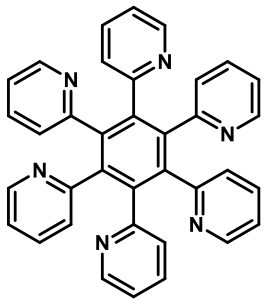

2

A microwave vial was loaded with 2-phenylpyridine (**1a**) (146 μL, 1 mmol) and 2-bromopyridine (760 μL, 8 mmol), $[RuCl_2(p\text{-cymene})]_2$ (60 mg, 0.1 mmol), PPh_3 (52 mg, 0.2 mmol), KOPiv (56 mg, 0,40 mmol), and Na_2CO_3 (1,040 mg, 10 mmol). The mixture was suspended in 2 mL of H_2O, bubbled with Ar for 3 min. The mixture was heated at 200 °C under microwave irradiation (max 100 W) for 4 h. The reaction mixture was then cooled to room temperature and diluted with 20 mL DCM and 20 mL H_2O. The product was extracted with DCM (2 x 20 mL). The combined organic phases were dried over anh. Na_2SO_4, filtrated and evaporated in vacuo. Crude product after extraction was triturated with EtOAc (20 mL), to obtain pure ligand **2** (519 mg, 97%) as a pale yellow solid. Analytical and spectroscopic data are in agreement with literature data [1].

Synthesis of 1,3,5-tri(pyridin-2-yl)benzene (1b)

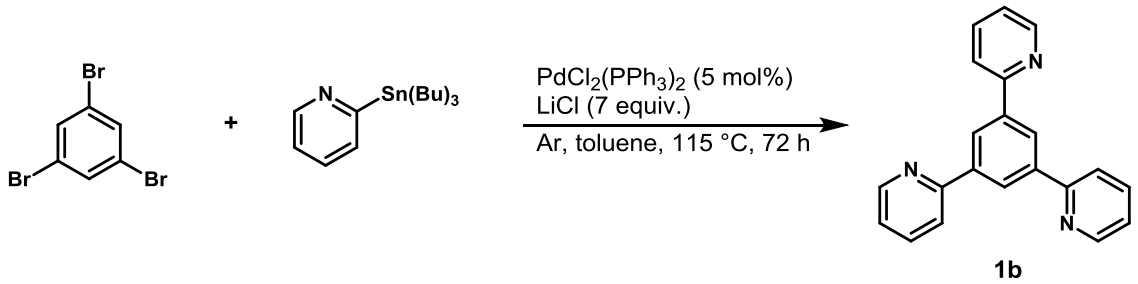

1b

Compound 2 was prepared by following slightly modified literature procedure for Stille reaction [2]. A mixture of 2-tri-n-butylstannylpyridine (1.17 mL, 3.5 mmol), 1,3,5-tribromobenzene (317 mg, 1 mmol), bis(triphenylphosphine)palladium(II) chloride (34 mg, 0.05 mmol) and lithium chloride (294 mg, 7 mmol) were suspended in dry toluene (3 mL) and degassed by five freeze-pump-thaw cycles. The reaction mixture was than stirred and heated under reflux at 115 °C for 72 h under Ar atmosphere. The solution was filtrated and residue was washed with toluene (3 mL). Saturated aqueous potassium fluoride solution (5 ml) was added and the resulting two-phase system was stirred for 30 min. The solid tin residue was removed by filtration and washed with toluene (3 x 3 mL). Phases were separated and the organic phase was dried over anh. Na_2SO_4, filtered and evaporated in vacuo. The crude product was triturated with petroleum ether and the precipitate was filtered off, washed with with Et_2O (2 x 5 mL) and dried to obtain compound **1b** (154 mg, 50%) as an orange solid. Analytical and spectroscopic data are in agreement with literature data [2].

2,2',2''-(2,4,6-Tri(pyridin-2-yl)benzene-1,3,5-triyl)triquinoline (3)

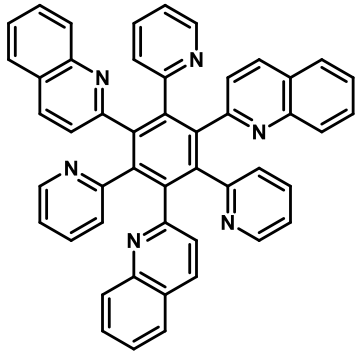

3

A microwave vial was loaded with 1,3,5-tri(pyridin-2-yl)benzene (**1b**) (77 mg, 0.25 mmol), 2-bromoquinoline (260 mg, 1.25 mmol), $[RuCl_2(p\text{-cymene})]_2$ (15 mg, 0.025 mmol), PPh_3 (13 mg, 0.05 mmol), KOPiv (14 mg, 0,10 mmol), and Na_2CO_3 (130 mg, 1,25 mmol). The mixture was suspended in 1 mL of H_2O, bubbled with Ar for 3 min and heated at 200 °C under microwave irradiation (max 100 W) for 4 h. The reaction mixture was then cooled to room temperature and diluted with 10 mL DCM and 10 mL H_2O. The product was extracted with DCM (2 x 10 mL). The combined organic phases were dried over anh. Na_2SO_4, filtered and evaporated in vacuo. The crude product was further purified by radial chromatography on silica gel using mixture of DCM and MeOH. (DCM/MeOH: 50/1 to 5/1) to obtain ligand **3** (150 mg, 87%) as a pale green solid. Analytical and spectroscopic data are in agreement with literature data [1].

The Synthesis of Complexes

$[Ag_4F(2)_2](OTf)_3$

A crew cap scintillation vial was loaded with ligand **2** (28 mg, 0.05 mmol), AgOTf (19.5 mg. 0.075 mmol) and AgF (3.4 mg, 0.025 mmol). The mixture was dissolved in 1 mL of MeOH and stirred in the dark at room temperature for 12 h. After that time Et_2O (2 mL) was added to precipitate the product, which was filtered off, washed with H_2O (1 mL) and Et_2O (2 x 1 mL) and dried to obtain the pure complex $[Ag_4F(\mathbf{2})_2](OTf)_3$ (38 mg, 0.0195 mmol, 78% yield) as a white solid. Mp. >300 °C (dec.). **^{1}H NMR** (500 MHz, acetone-d_6): δ = 8.10 (d, *J* = 5.0 Hz, 1H), 7.91 (d, *J* = 7.9 Hz, 1H), 7.74 (td, *J* = 7.7, 1.7 Hz, 1H), 7.17 (ddd, *J* = 7.6, 5.1, 1.3 Hz, 1H). **^{13}C NMR** (126 MHz, acetone-d_6): δ = 157.8, 150.3, 141.4, 138.7, 128.5, 124.1 121.6 (q, *J* = 322.0 Hz). **^{19}F NMR** (471 MHz, acetone-d_6): *δ* –78.6 (OTf), –315.9 (F^-). **IR** (ATR): 1592, 1566, 1483, 1405, 1256, 1221, 1151, 1027, 997, 806, 754, 635 cm^{-1}. **HR-MS** (ESI) m/z calcd for $C_{72}H_{48}N_{12}FAg_4$ $[M\text{-}3OTf]^{3+}$: 509.0099, found: 509.0100. **Elemental analysis** calcd (%) for $C_{75}H_{48}Ag_4F_{10}N_{12}O_9S_3\times3H_2O$: C 44.31, H 2.68, N 8.27; found: C 44.25, H 2.45, N 8.19.

$[Ag_4F(3)_2](OTf)_3$

A crew cap scintillation vial was loaded with ligand **3** (34,5 mg, 0.05 mmol), AgOTf (19.5 mg. 0.075 mmol) and AgF (3.4 mg, 0.025 mmol). The mixture was dissolved in 1 mL of MeOH and stirred in the dark at room temperature for 12 h. After that time Et_2O (2 mL) was added to precipitate the product, which was filtered off, washed with H_2O (1 mL) and Et_2O (2 x 1 mL) and dried to obtain the pure complex $[Ag_4F(\mathbf{3})_2](OTf)_3$ (40 mg, 0.018 mmol, 71% yield) as a white solid. Mp. >300 °C (dec.). **^{1}H NMR** (500 MHz, acetone-d_6): δ = 8.38 (d, *J* = 8.5 Hz, 1H), 8.27 (d, *J* = 8.5 Hz, 1H), 8.16 (dt, *J* = 7.9, 1.1 Hz, 1H), 8.03 (d, *J* = 5.0 Hz, 1H), 7.84 (d, *J* = 7.9 Hz, 1H), 7.26 (ddd, *J* = 8.0, 6.9, 1.2 Hz, 1H), 7.01 (ddd, *J* = 7.6, 5.1, 1.3 Hz, 1H), 6.71 (d, *J* = 8.7 Hz, 1H), 6.52 (ddd, *J* = 8.5, 6.9, 1.3 Hz, 1H). **^{13}C NMR** (126 MHz, acetone-d_6): δ = 159.9, 158.1, 150.5, 146.2, 142.3, 141.5, 139.1, 139.0, 130.5, 129.0, 128.9, 128.5, 128.3, 127.8, 125.5, 124.3 121.6 (q, *J* = 322.0 Hz). **^{19}F NMR** (471 MHz,

acetone-d_6): δ –78.6 (OTf), –312.3 (F^-). **IR** (ATR): 1604, 1569, 1327, 1259, 1165, 1122, 1078, 1029, 1020, 868, 729, 637 cm^{-1}. **ESI-MS** m/z for $C_{96}H_{60}Ag_4FN_{12}$ $[M\text{-}3OTf]^{3+}$: 610.4. **Elemental analysis** calcd (%) for $C_{99}H_{60}Ag_4F_{10}N_{12}O_9S_3$: C 52.17, H 2.65, N 7.37; found: C 46.00, H 2.35, N 6.16.

$[Ag_5F(2)_2](OTf)_4$

A screw cap scintillation vial was loaded with ligand **2** (28 mg, 0.05 mmol), AgOTf (32,5 mg. 0.125 mmol) and AgF (3.4 mg, 0.025 mmol). The mixture was dissolved in 1 mL of MeOH and stirred in the dark at room temperature for 12 h. After that time Et_2O (2 mL) was added to precipitate the product, which was filtered off, washed with H_2O (1 mL) and Et_2O (2 x 1 mL) and dried to obtain the pure complex $[Ag_5F(\mathbf{2})_2](OTf)_4$ (40 mg, 0.0215 mmol, 86% yield) as a white solid. Mp. >300 °C (dec.). **^{1}H NMR** (500 MHz, acetone-d_6): δ = 8.38 (d, J = 5.1 Hz, 1H), 8.15 (dt, J = 7.9, 1.2 Hz, 1H), 7.89 (td, J = 7.8, 1.6 Hz, 1H), 7.32 (ddd, J = 7.7, 5.2, 1.3 Hz, 1H). **^{13}C NMR** (126 MHz, acetone-d_6): δ = 157.3, 152.1, 141.9, 140.2, 129.7, 125.2 121.3 (q, J = 321.2 Hz). **^{19}F NMR** (471 MHz, acetone-d_6): δ –78.7 (OTf), –284.5 (F^-). **IR** (ATR): 1592, 1565, 1434, 1405, 1258, 1221, 1150, 1028, 997, 806, 754, 635 cm^{-1}. **ESI-MS** m/z for $C_{72}H_{48}Ag_4FN_{12}$ $[M\text{-}Ag^+\text{-}3OTf]^{3+}$: 510.3. **Elemental analysis** calcd (%) for $C_{76}H_{48}Ag_5F_{13}N_{12}O_{12}S_4 \times C_6H_6$: C 42.56, H 2.35, N 7.26; found: C 42.85, H 2.40, N 7.86.

$[Ag_4F(2)_2](PF_6)_3$

A screw cap scintillation vial was loaded with ligand **2** (28 mg, 0.05 mmol), $AgPF_6$ (19 mg. 0.075 mmol) and AgF (3.4 mg, 0.025 mmol). The mixture was dissolved in 1 mL of MeOH and stirred in the dark at room temperature for 12 h. After that time Et_2O (2 mL) was added to precipitate the product, which was filtered off, washed with H_2O (1 mL) and Et_2O (2 x 1 mL) and dried to obtain the pure complex $[Ag_4F(\mathbf{2})_2](PF_6)_3$ (48 mg, 0.0205 mmol, 82% yield) as a white solid. Mp. >300 °C (dec.). **^{1}H NMR** (500 MHz, acetone-d_6): δ = 8.14 (d, J = 5.1 Hz, 1H), 7.78 (td, J = 7.6, 1.6 Hz, 1H), 7.74 (dt, J = 7.7, 1.3 Hz, 1H), 7.21 (ddd, J = 7.4, 5.0, 1.5 Hz, 1H). **^{13}C NMR** (126 MHz, acetone-d_6): δ = 156.5, 149.8, 140.8, 138.1, 127.3, 123.4. **^{19}F NMR** (471 MHz, acetone-d_6): δ –72.5 (d, $^1J_{FP}$ = 708.2 Hz, PF_6^-), –316.0 (F^-). **IR** (ATR): 1593, 1486, 1404, 875, 836, 807, 754 cm^{-1}. **Elemental analysis** calcd (%) for $C_{72}H_{48}Ag_4F_{19}N_{12}P_3 \times 2H_2O$: C 43.18, H 2.63, N 8.39; found: C 42.89, H 2.30, N 8.29.

$[Ag_4F(2)_2](SbF_6)_3$

A screw cap scintillation vial was loaded with ligand **2** (28 mg, 0.05 mmol), $AgSbF_6$ (26 mg. 0.075 mmol) and AgF (3.4 mg, 0.025 mmol). The mixture was dissolved in 1 mL of MeOH and stirred in the dark at room temperature for 12 h. After that time Et_2O (2 mL) was added to precipitate the product, which was filtered off, washed with H_2O (1 mL) and Et_2O (2 x 1 mL) and dried to obtain the pure complex $[Ag_4F(\mathbf{2})_2](SbF_6)_3$ (45 mg, 0.02 mmol, 80% yield) as a white solid. Mp. >300 °C (dec.). **^{1}H NMR** (500 MHz, acetone-d_6): δ = 8.14 (d, J = 5.0 Hz, 1H), 7.86–7.70 (m, 2H), 7.21 (ddd, J = 7.4, 5.1, 1.5 Hz, 1H). **^{19}F NMR** (471 MHz, acetone-d_6): δ –123.2 (superposition of a sextet due to $^{121}SbF_6^-$ and an octet due to $^{123}SbF_6^-$, $^1J_F{}^{121}_{Sb}$ = 1941, $^1J_F{}^{123}_{Sb}$ = 1051 Hz), –316.4 (F^-). **^{13}C NMR** (126 MHz, acetone-d_6): δ = 157.3, 150.7, 141.8, 139.0, 128.2, 124.3. **IR** (ATR): 1592, 1565, 1484, 1405, 997, 807, 753, 654 cm^{-1}. **Elemental analysis** calcd (%) for $C_{72}H_{48}Ag_4F_{19}N_{12}Sb_3$: C 38.61, H 2.16, N 7.51; found: C 38.50, H 2.08, N 7.44.

Synthesis of Complex $[Ag_5F(2)_2](OTf)_4$ from $[Ag_4F(2)_2](OTf)_3$. A screw cap scintillation vial was loaded with complex $[Ag_4F(\mathbf{2})_2](OTf)_3$ (10 mg, 0.005 mmol) and AgOTf (3.8 mg. 0.0125 mmol). The mixture was dissolved in 0.5 mL of MeOH and stirred in the dark at room temperature for 12 h. After that time Et_2O (1 mL) was added to precipitate the product, which was filtered off, washed with H_2O (0.5 mL) and Et_2O (2 x 0.5 mL) and dried to obtain the complex $[Ag_5F(\mathbf{2})_2](OTf)_4$ (6.8 mg, 0.003 mmol, 61%) as a white solid.

Synthesis of Complex $[Ag_4F(2)_2](OTf)_3$ from $[Ag_5F(2)_2](OTf)_4$. A screw cap scintillation vial was loaded with complex $[Ag_5F(\mathbf{2})_2](OTf)_4$ (12 mg, 0.005 mmol), which was suspended in 1 mL of H_2O and stirred in the dark at room temperature for 0.5 h. After that time the product was filtered off, and washed with H_2O (0.5 mL) and Et_2O (2 x 0.5 mL) and dried to obtain the pure complex $[Ag_4F(\mathbf{2})_2](OTf)_3$ (7 mg, 0.0036 mmol, 72%) as a white solid.

Synthesis of Complex $[Ag_4F(2)_2](OTf)_3$ from $[Ag_5F(2)_2](OTf)_4$. A screw cap scintillation vial was loaded with complex $[Ag_5F(\mathbf{2})_2](OTf)_4$ (11 mg, 0.005 mmol), ligand **2** (1.4 mg, 0.0025 mmol) and KF (14.5 mg, 0.25 mmol). The mixture was suspended in 0.5 mL of MeOH and stirred in the dark at room temperature for 12 h. After that time Et_2O (1 mL) was added to precipitate the product, which was filtered off, washed with H_2O (0.5 mL) and Et_2O (2 x 0.5 mL) and dried to obtain the complex $[Ag_4F(\mathbf{2})_2](OTf)_3$ (10 mg, 0.005 mmol, 80%) as a white solid.

Dissociation of Complex $[Ag_4F(2)_2](OTf)_3$ with NaCl. A screw cap scintillation vial was loaded with complex $[Ag_4F(\mathbf{2})_2](OTf)_3$ (20 mg, 0.01 mmol) and NaCl (5,8 mg, 0.1 mmol). The mixture was suspended in 1 mL of MeOH and stirred in the dark at room temperature for 12 h. After that time MeOH was evaporated in vacuo. The crude product was suspended in DCM (2 mL), filtered and filtrate was evaporated to obtain the pure ligand **2** (8 mg, 0.015 mmol, 80%) as a white solid.

Proportions of complexes $[Ag_4F(2)_2](OTf)_3$ and $[Ag_5F(2)_2](OTf)_4$ in crude reaction mixture as a function of different [Ag(I)]/[2] ratios

Screw cap scintillation vial was loaded with ligand **2** (28 mg, 0.05 mmol), AgF (3.4 mg, 0.025 mmol) and AgOTf (0.075–0.125 mmol). The mixture was dissolved in 1 mL MeOH and stirred in the dark at room temperature for 12 h. After that, MeOH was evaporated in vacuo and the crude reaction mixture was analysed by ^{1}H NMR spectroscopy in acetone-d_6.

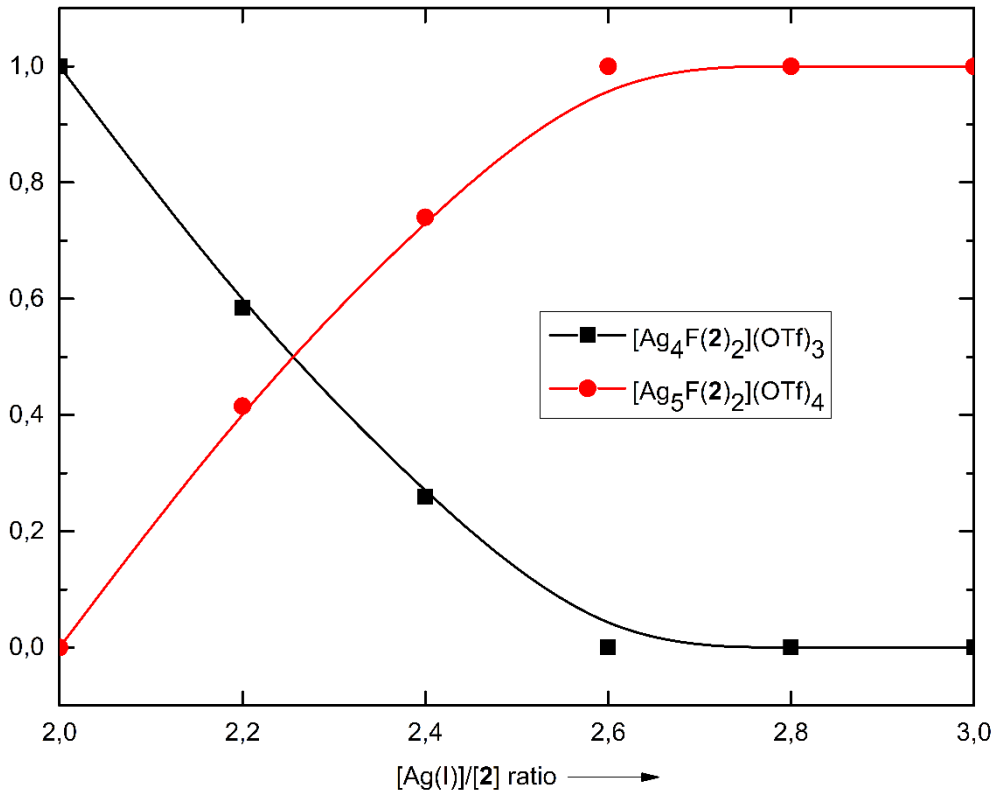

Figure S1: Proportions of Ag(I) complexes in crude reaction mixtures as a function of different [Ag(I)]/[**2**] ratios, determined by ^{1}H NMR spectroscopy.

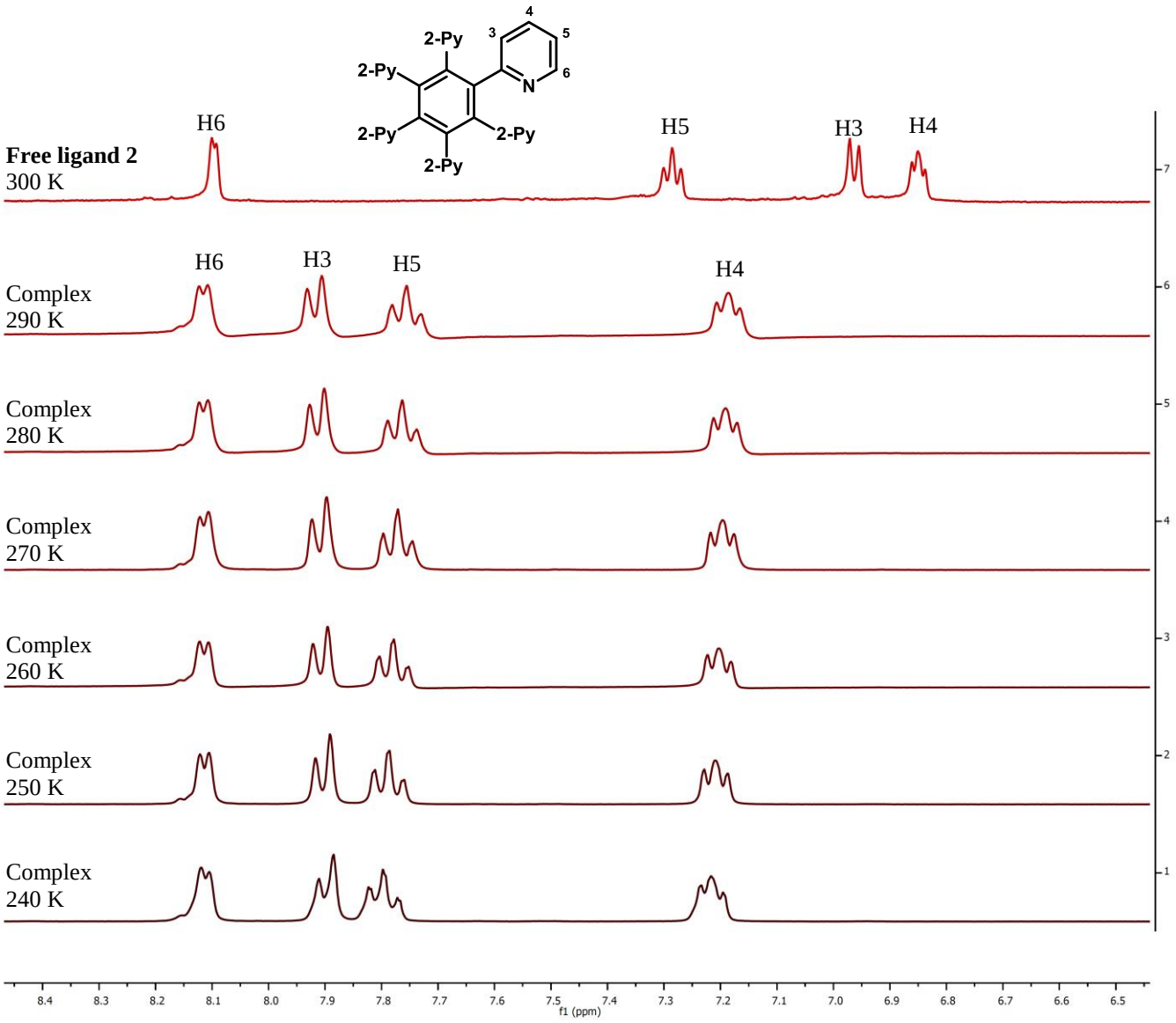

Figure S2: Stacked ^{1}H NMR (300 MHz, acetone-d_6) spectra of the complex $[Ag_4F(\mathbf{2})_2](OTf)_3$ and free ligand **2** at different temperatures (240–300 K).

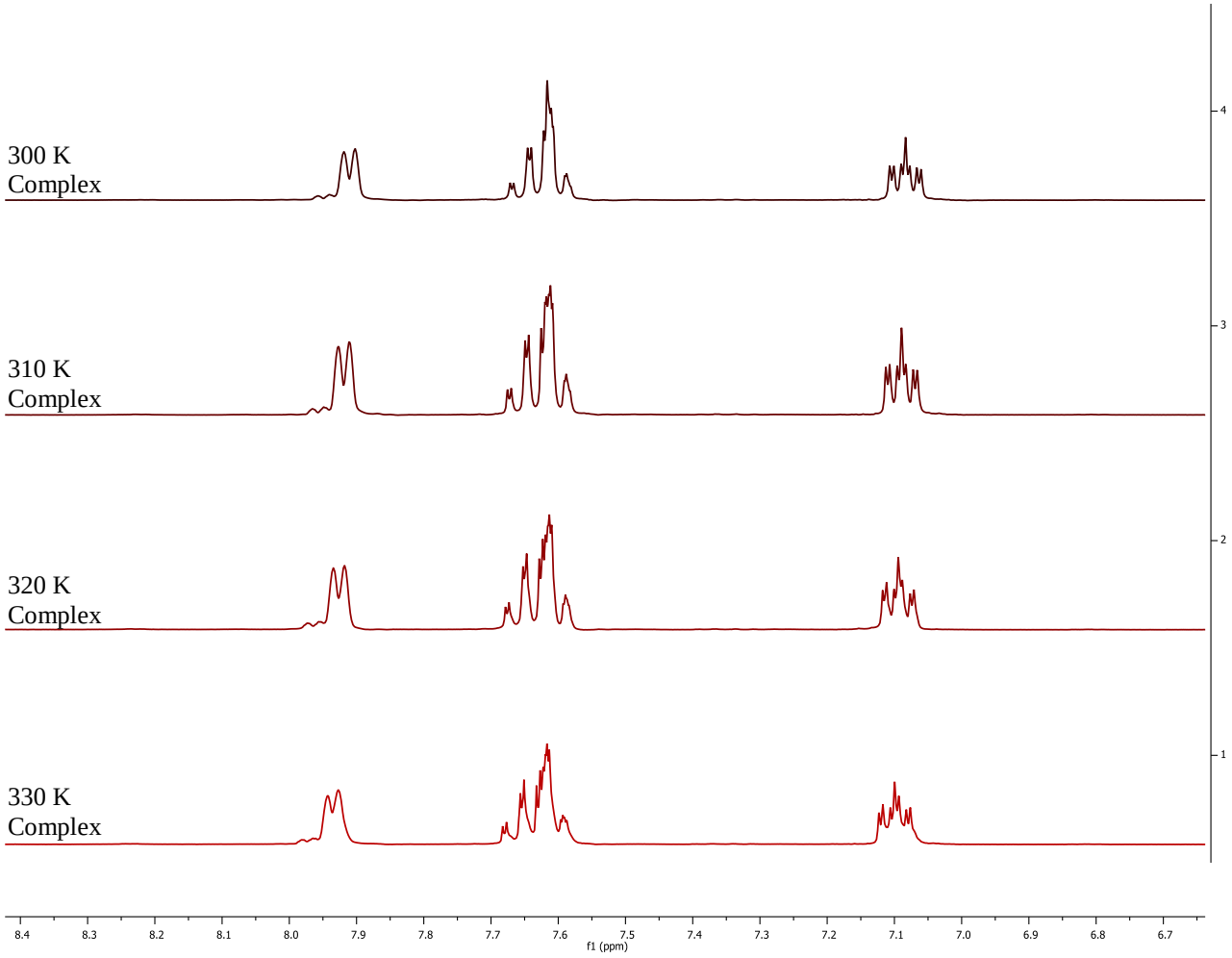

Figure S3: Stacked ^{1}H NMR (300 MHz, CD_3CN) spectra of the complex $[Ag_4F(\mathbf{2})_2](OTf)_3$ upon heating (300–330 K).

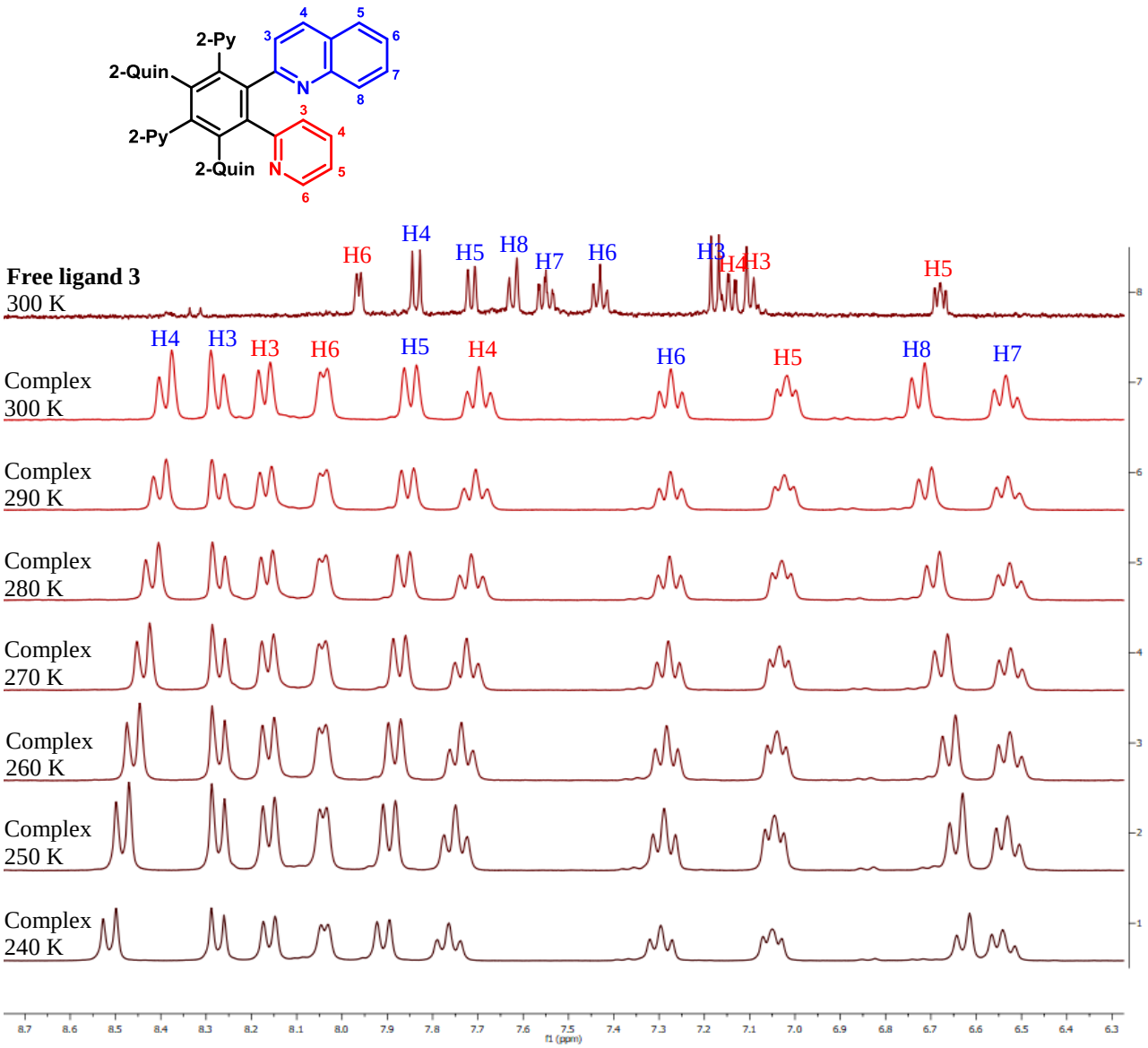

Figure S4: Stacked ^{1}H NMR (300 MHz, acetone-d_6) spectra of the complex $[Ag_4F(\mathbf{3})_2](OTf)_3$ and free ligand **3** at different temperatures (240–300 K).

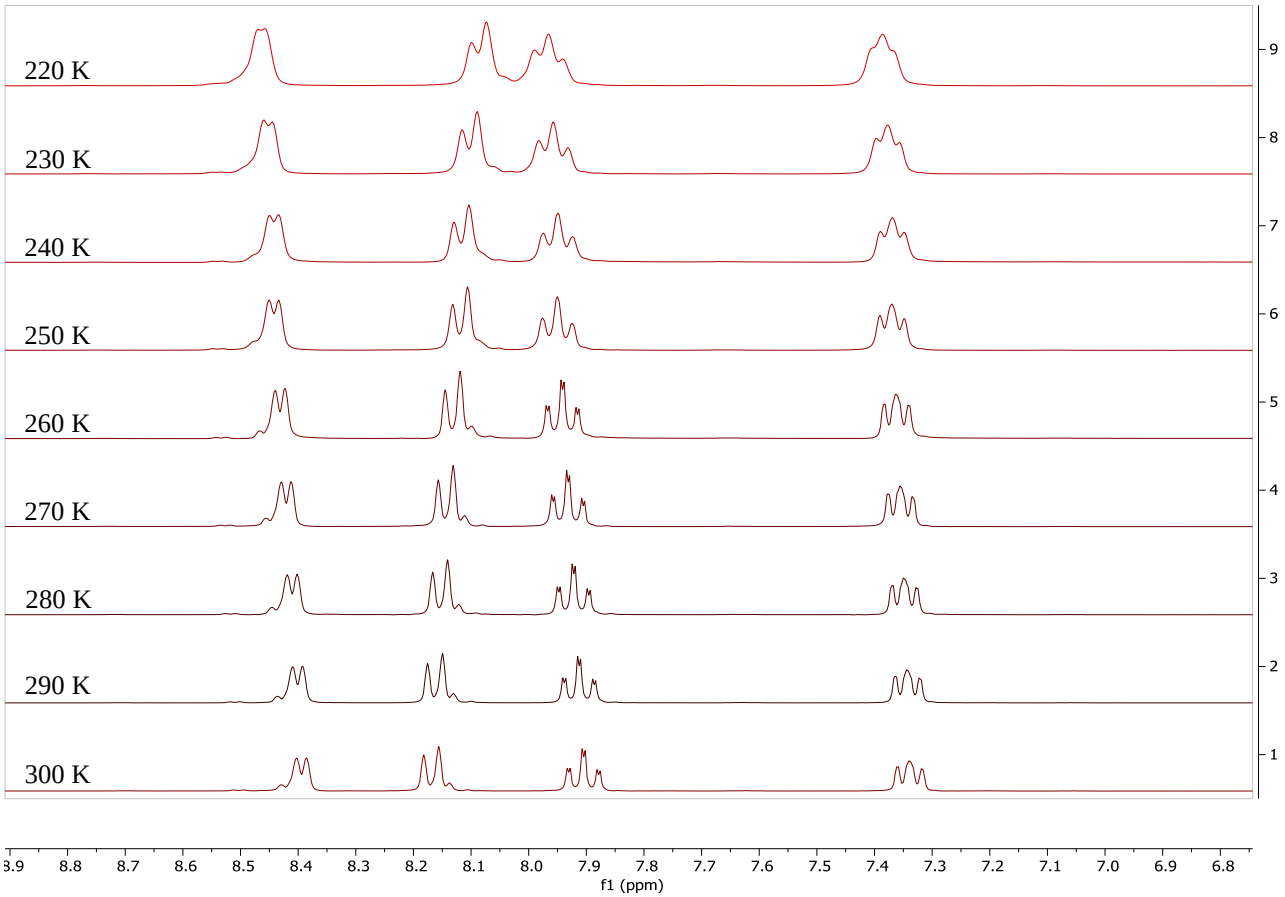

Figure S5: Stacked ^{1}H NMR (300 MHz, acetone-d_6) spectra of the complex $[Ag_5F(\mathbf{2})_2](OTf)_4$ at different temperatures (220–300 K).

NMR spectra

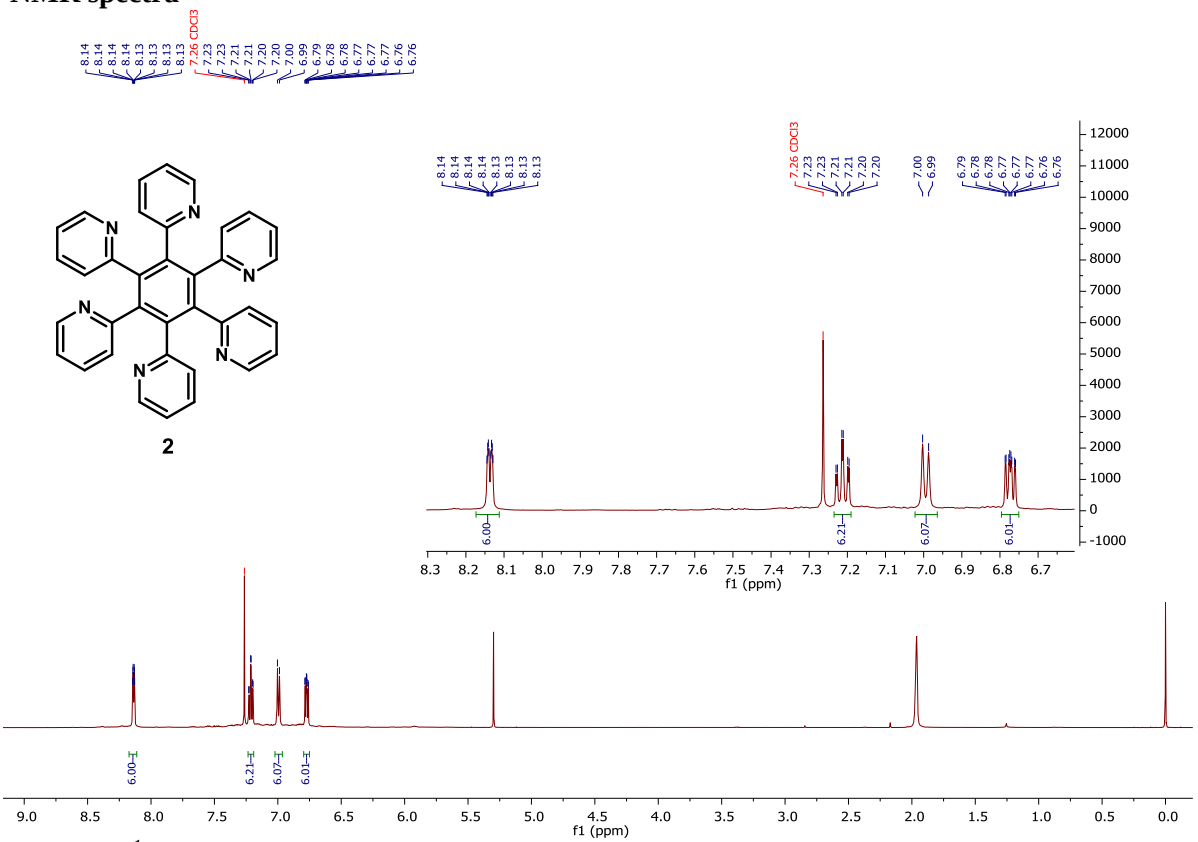

Figure S6: ^{1}H NMR spectrum (500 MHz) of ligand **2** in $CDCl_3$ at 296 K.

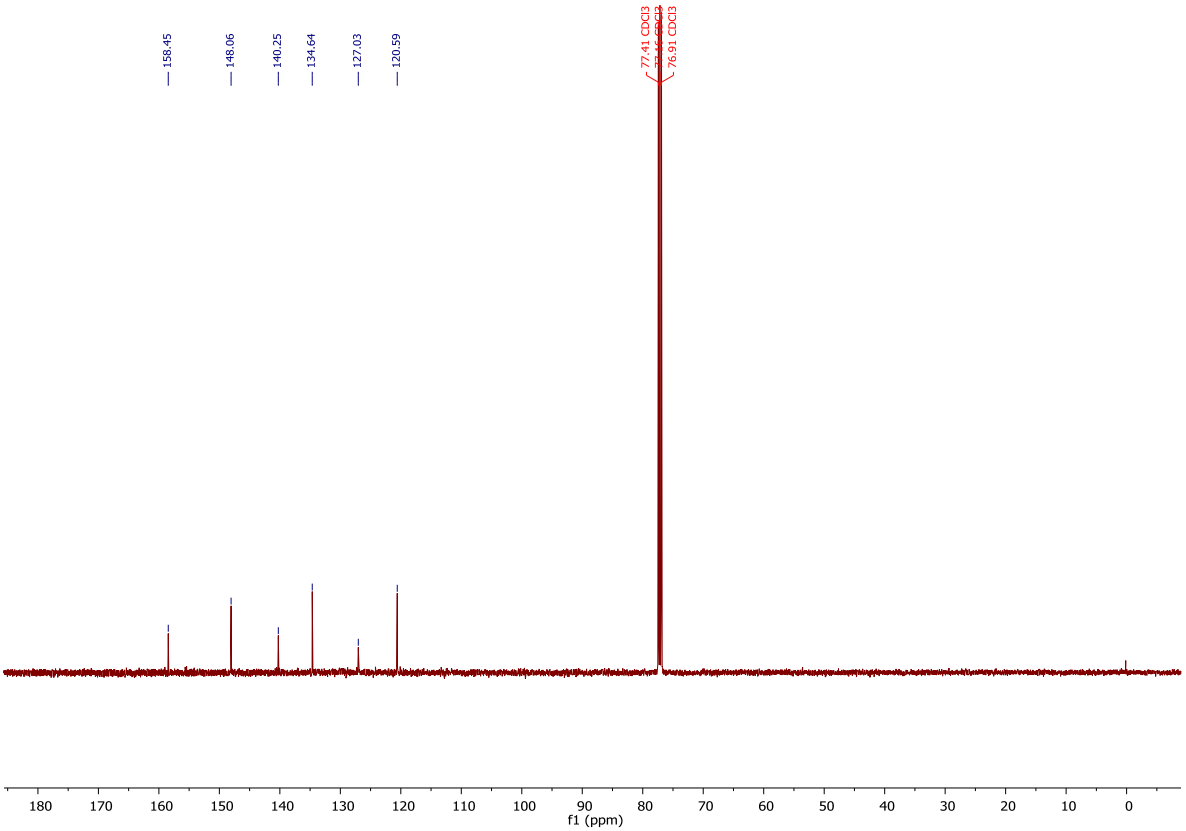

Figure S7: ^{13}C NMR spectrum (126 MHz) of ligand **2** in $CDCl_3$ at 296 K.

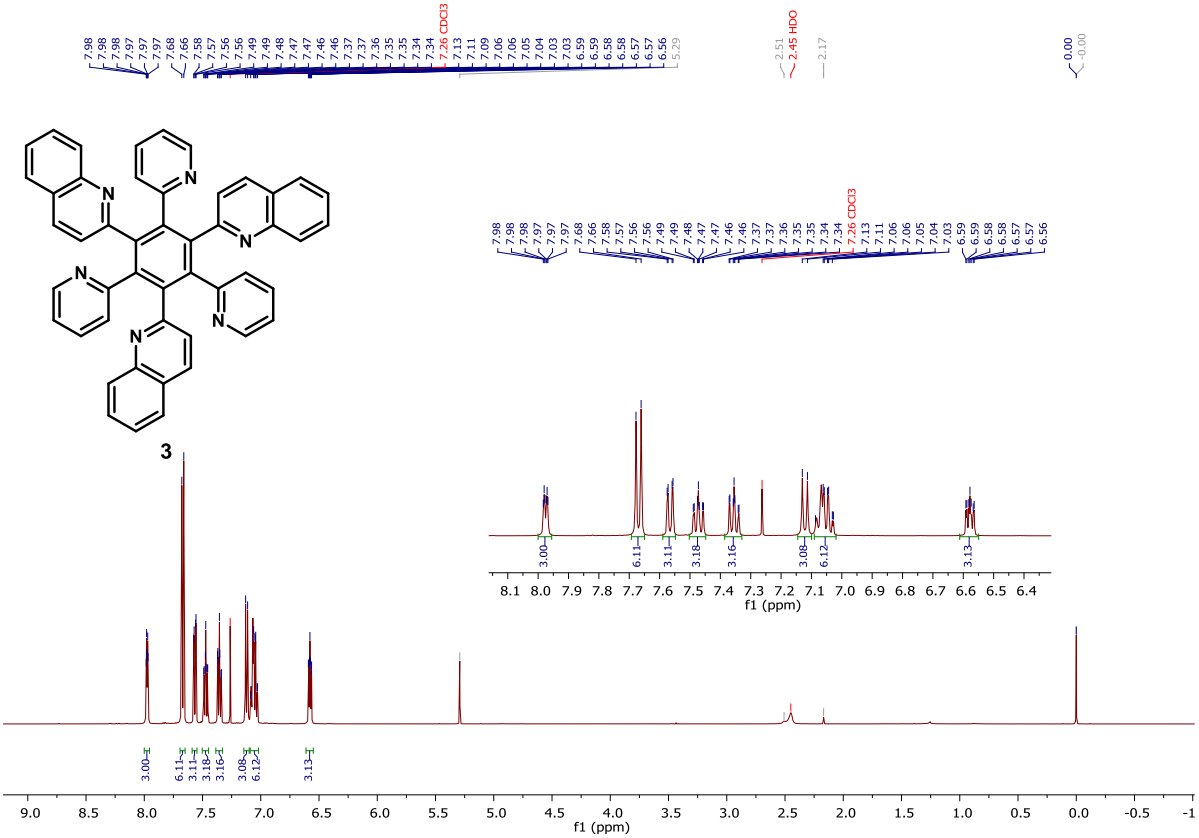

Figure S8: ^{1}H NMR spectrum (500 MHz) of ligand **3** in $CDCl_3$ at 296 K.

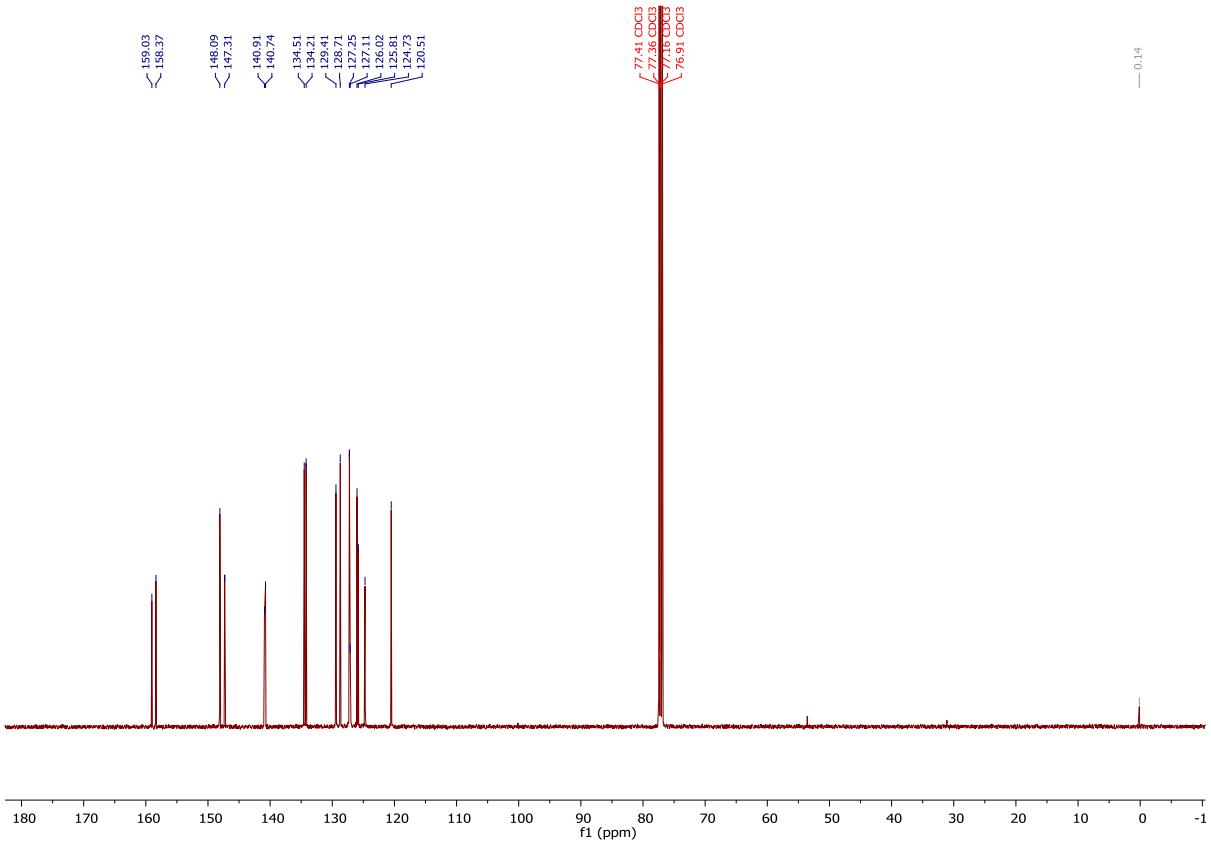

Figure S9: ^{13}C NMR spectrum (126 MHz) of ligand **3** in $CDCl_3$ at 296 K.

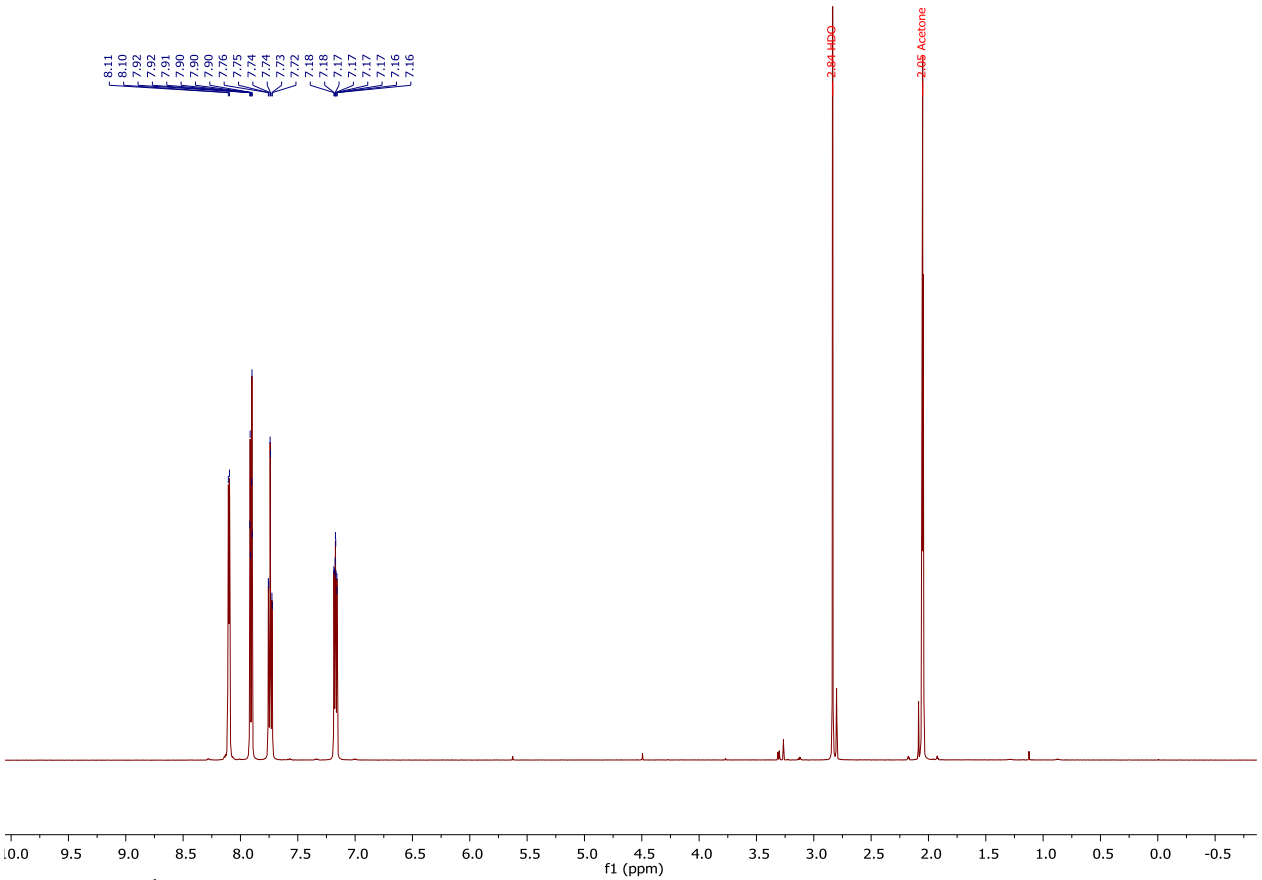

Figure S10: ^{1}H NMR spectrum (500 MHz) of $[Ag_4F(\mathbf{2})_2](OTf)_3$ in acetone-d_6 at 296 K.

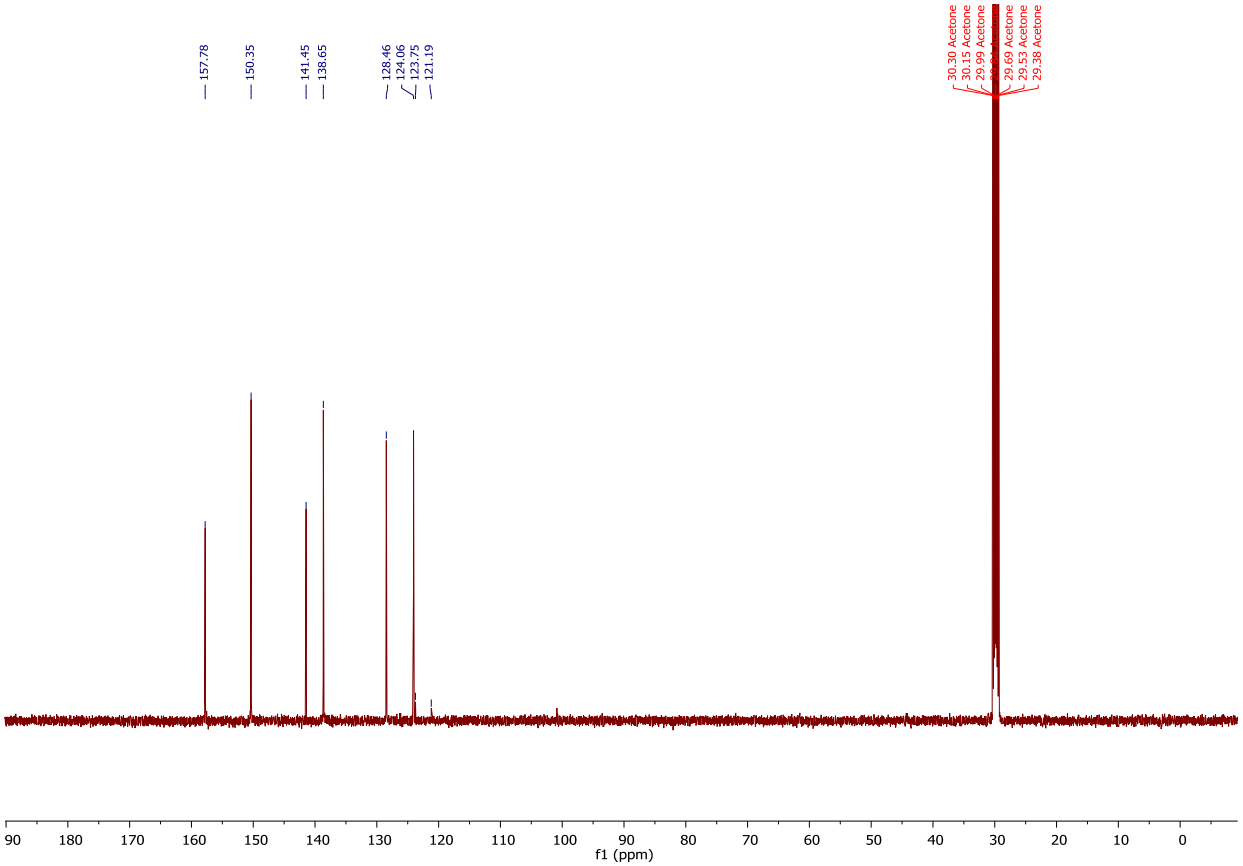

Figure S11: ^{13}C NMR spectrum (126 MHz) of $[Ag_4F(\mathbf{2})_2](OTf)_3$ in acetone-d_6 at 296 K.

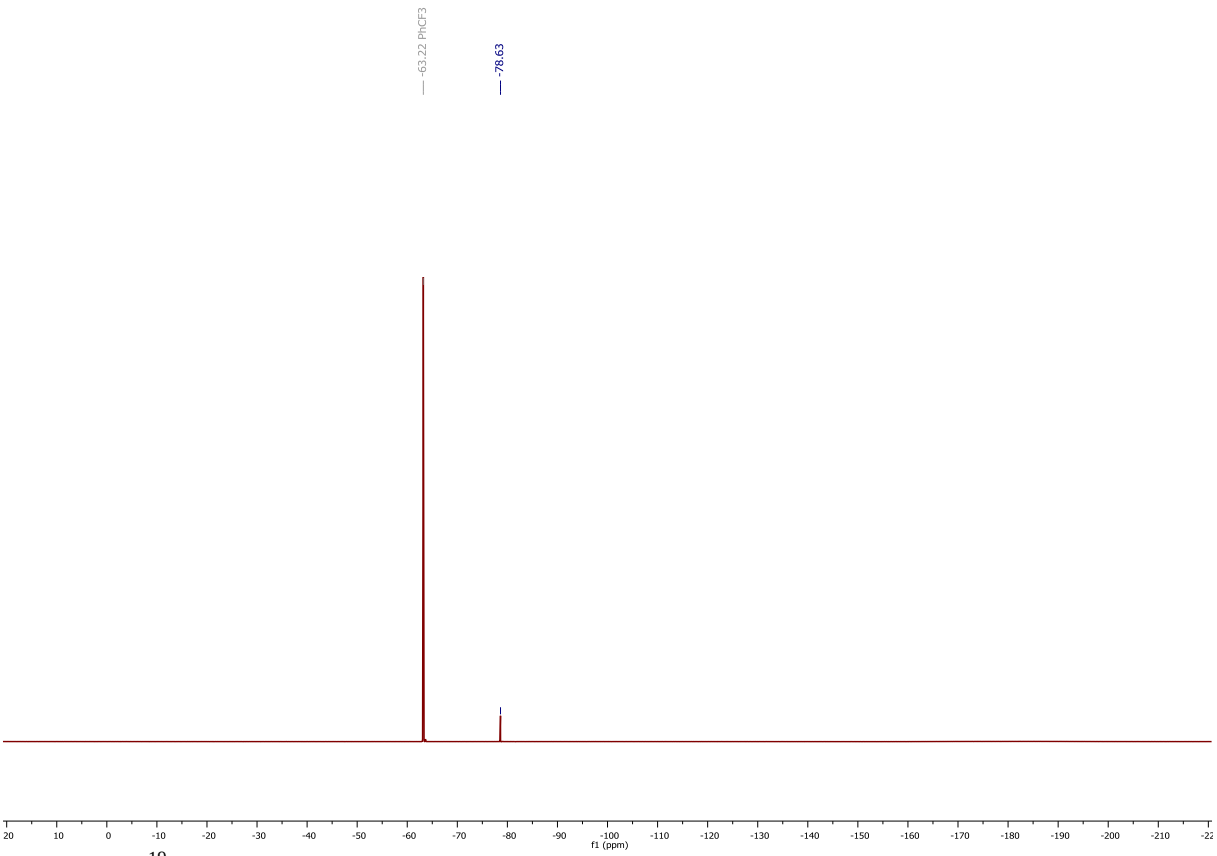

Figure S12: ^{19}F NMR spectrum (471 MHz) of $[Ag_4F(\mathbf{2})_2](OTf)_3$ in acetone-d_6 at 296 K (spectral window from 20 to –220 ppm) showing signal for OTf (signal at –63.2 corresponds to $PhCF_3$).

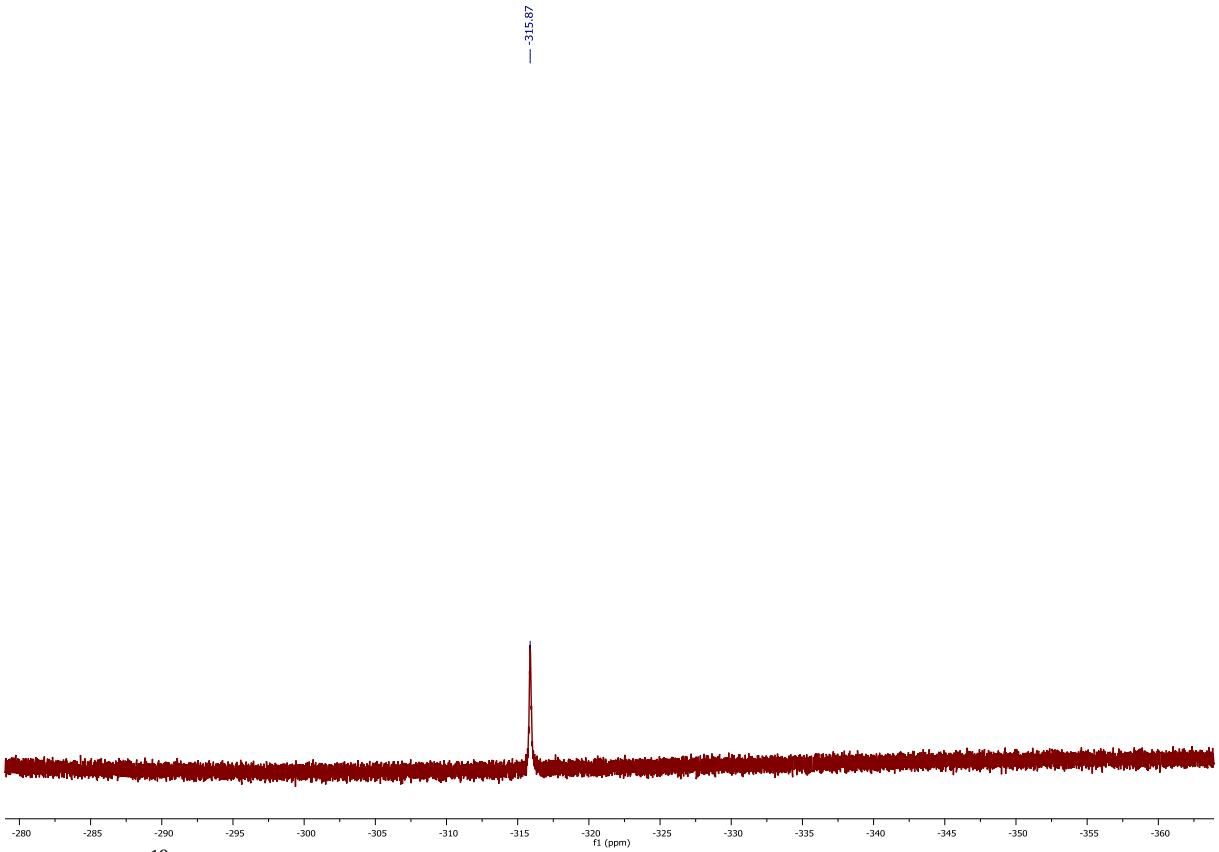

Figure S13: ^{19}F NMR spectrum (471 MHz) of $[Ag_4F(\mathbf{2})_2](OTf)_3$ in acetone-d_6 at 296 K (spectral window from –230 to –470 ppm) showing signal for F^-.

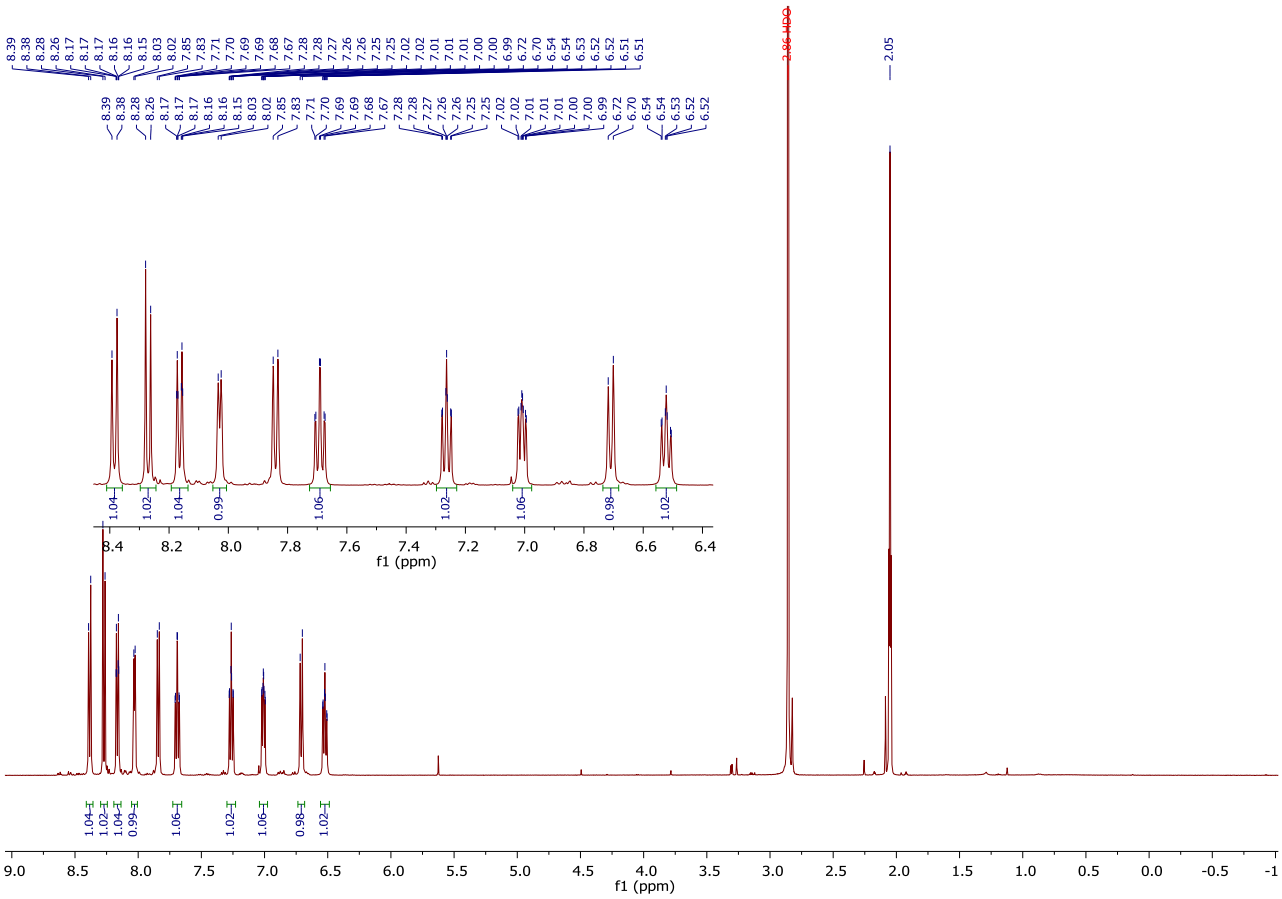

Figure S14: ^{1}H NMR spectrum (500 MHz) of $[Ag_4F(\mathbf{3})_2](OTf)_3$ in acetone-d_6 at 296 K.

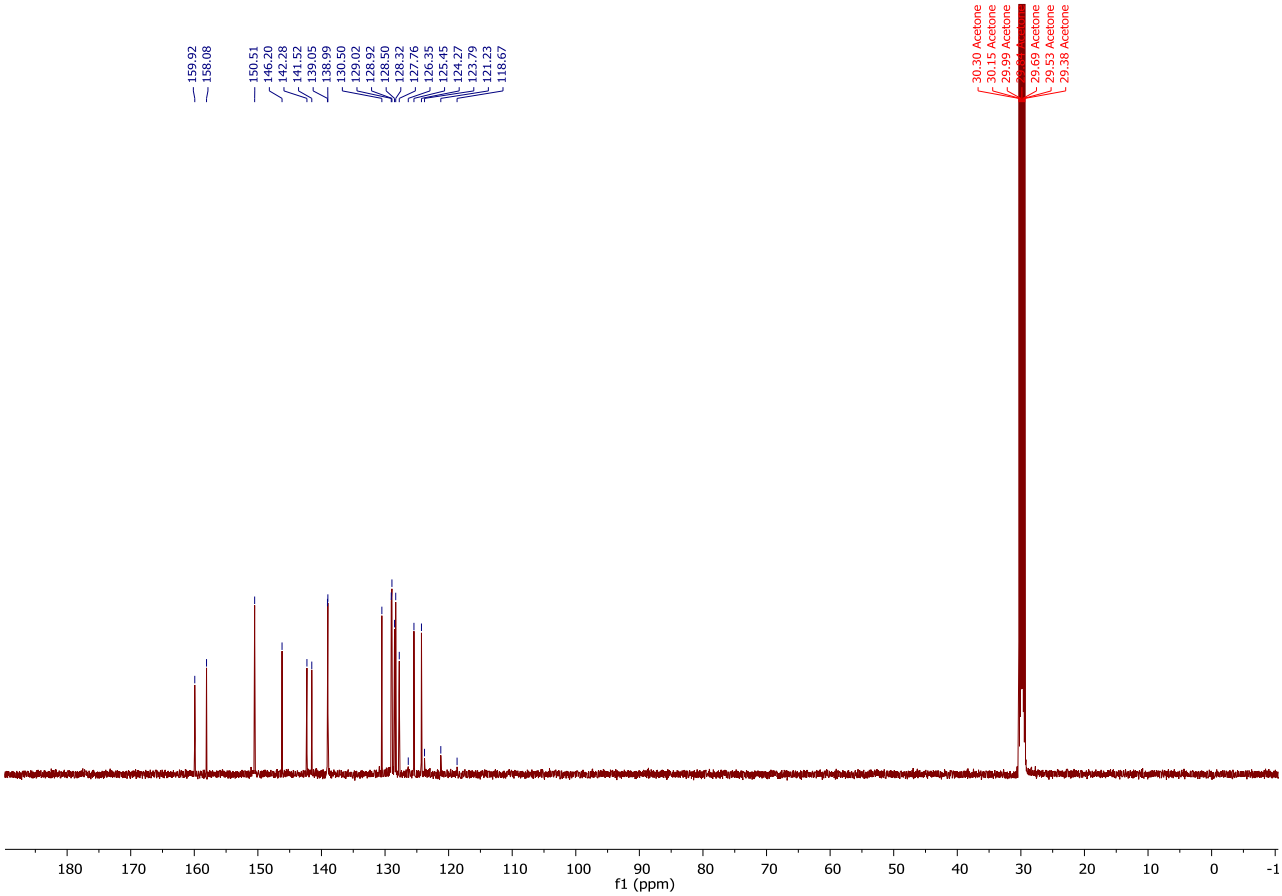

Figure S15: ^{13}C NMR spectrum (126 MHz) of $[Ag_4F(\mathbf{3})_2](OTf)_3$ in acetone-d_6 at 296 K.

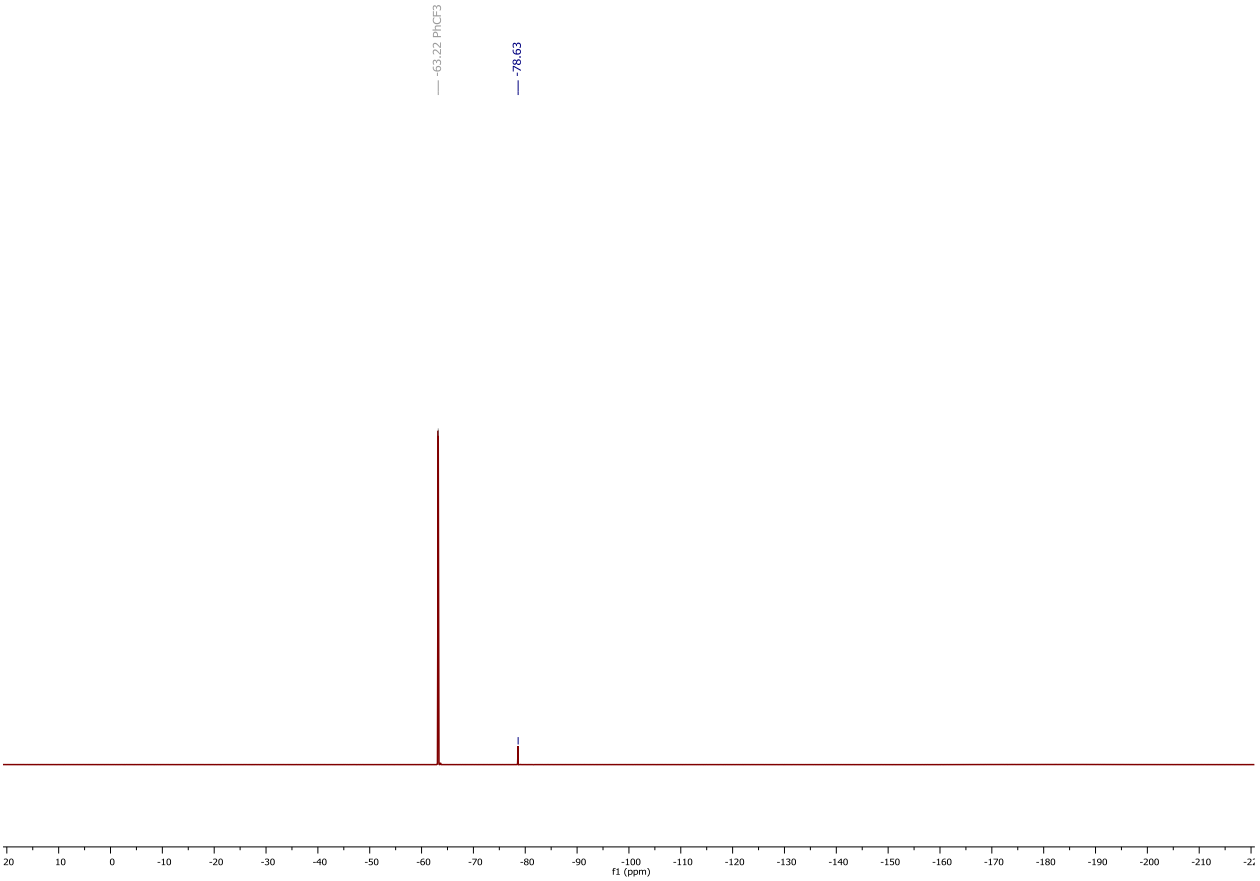

Figure S16: ^{19}F NMR spectrum (471 MHz) of $[Ag_4F(\mathbf{3})_2](OTf)_3$ in acetone-d_6 at 296 K (spectral window from 20 to –220 ppm) showing signal for OTf (signal at –63.2 corresponds to $PhCF_3$).

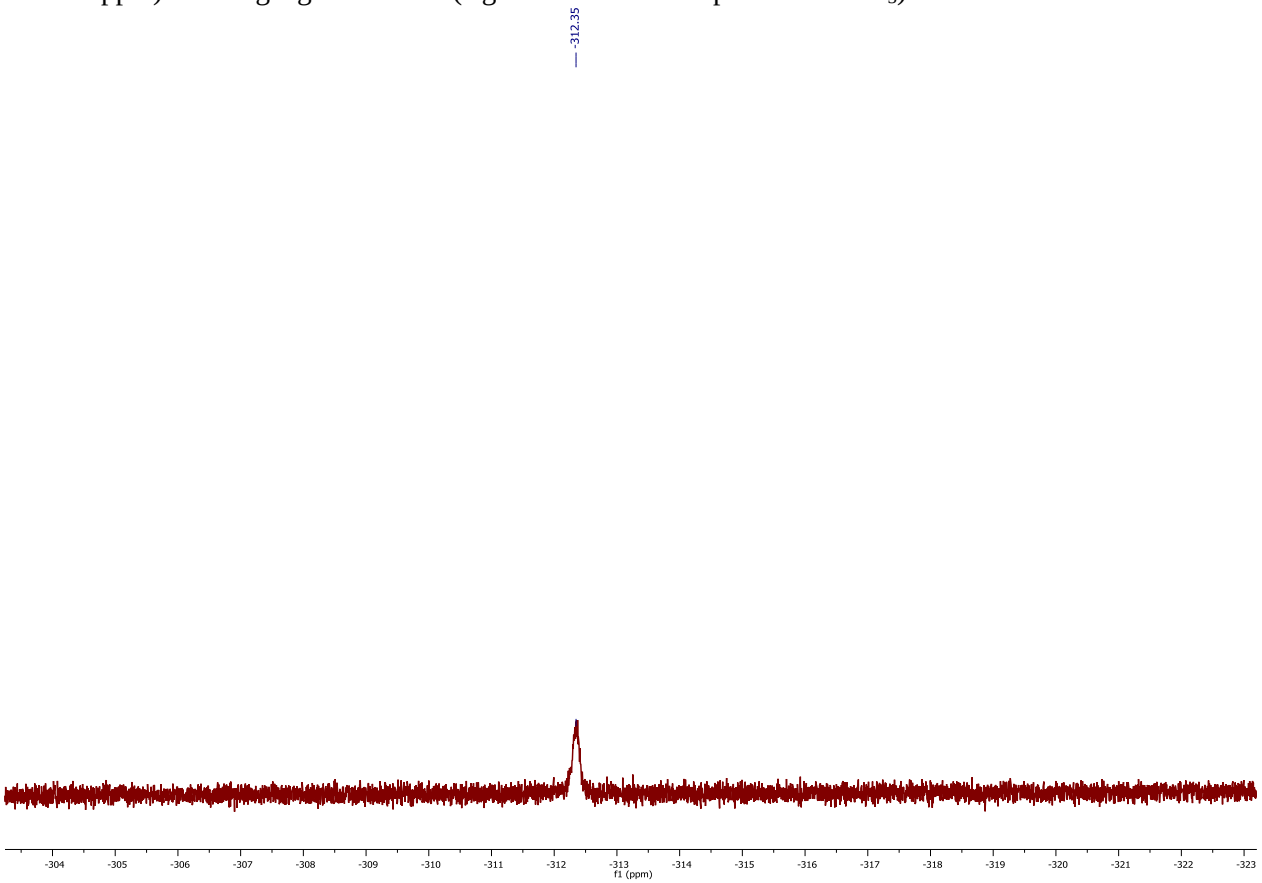

Figure S17: ^{19}F NMR spectrum (471 MHz) of $[Ag_4F(\mathbf{3})_2](OTf)_3$ in acetone-d_6 at 296 K (spectral window from –230 to –470 ppm) showing signal for F^-.

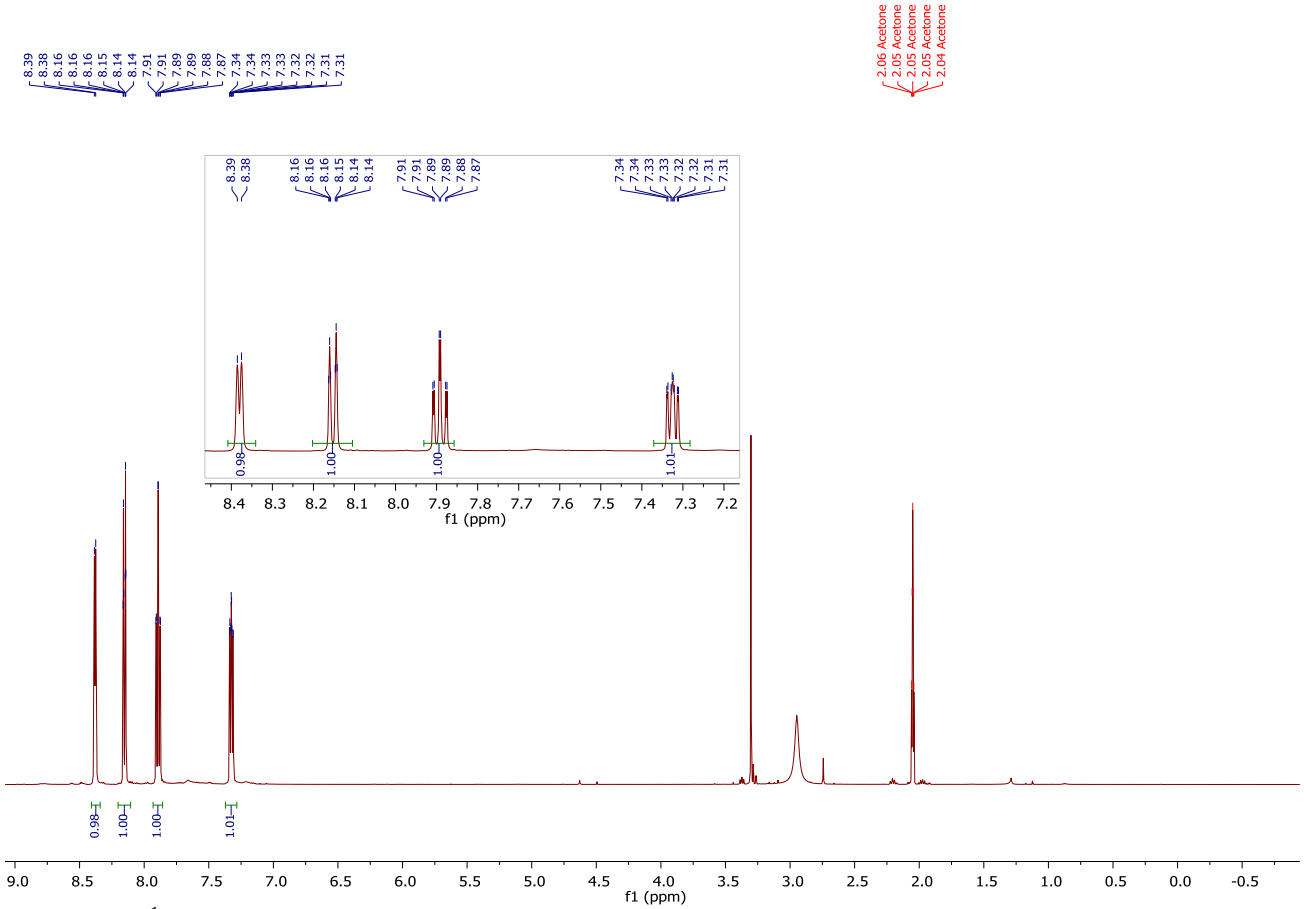

Figure S18: ^{1}H NMR spectrum (500 MHz) of $[Ag_5F(\mathbf{2})_2](OTf)_4$ in acetone-d_6 at 296 K.

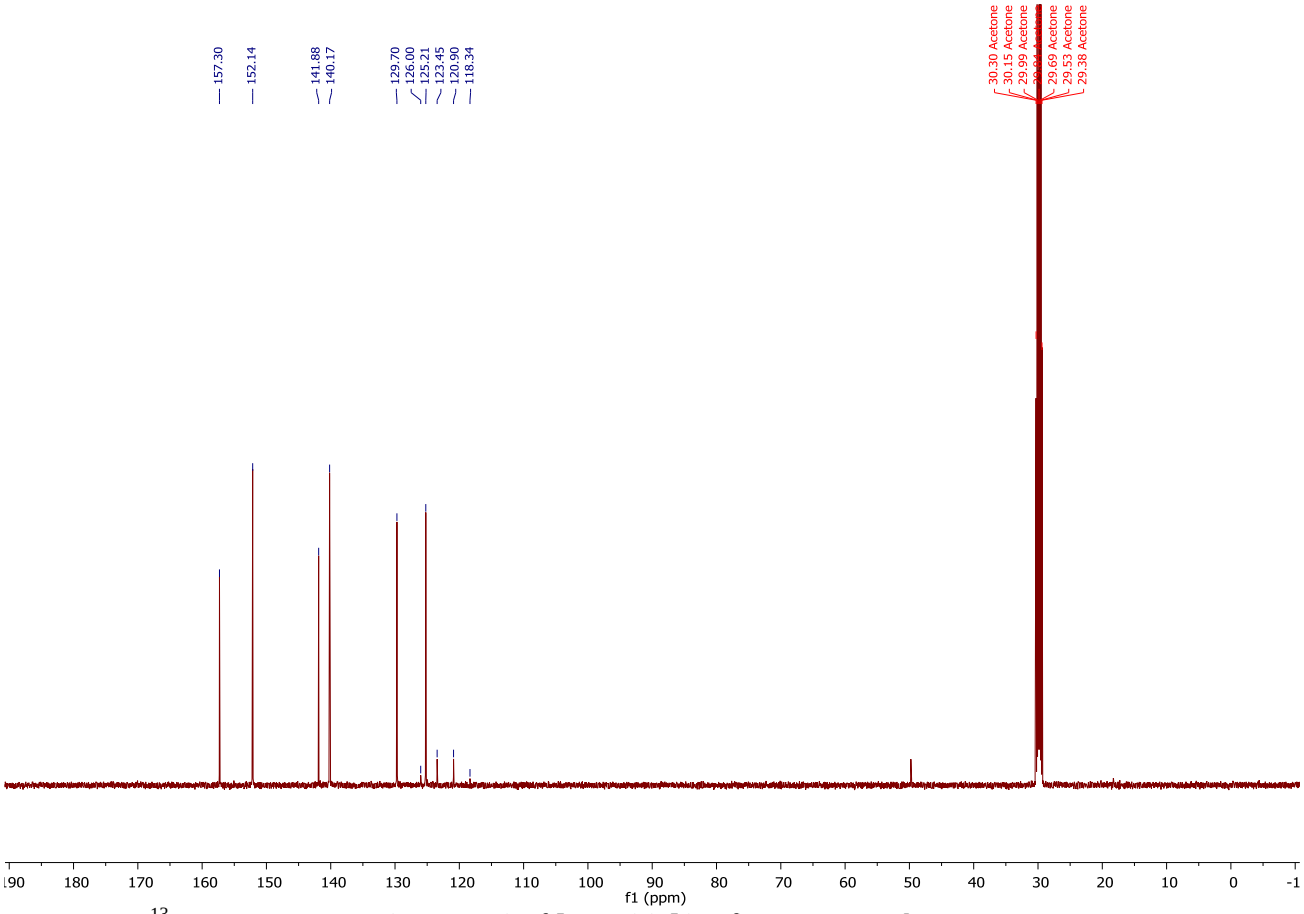

Figure S19: ^{13}C NMR spectrum (126 MHz) of $[Ag_5F(\mathbf{2})_2](OTf)_4$ in acetone-d_6 at 296 K.

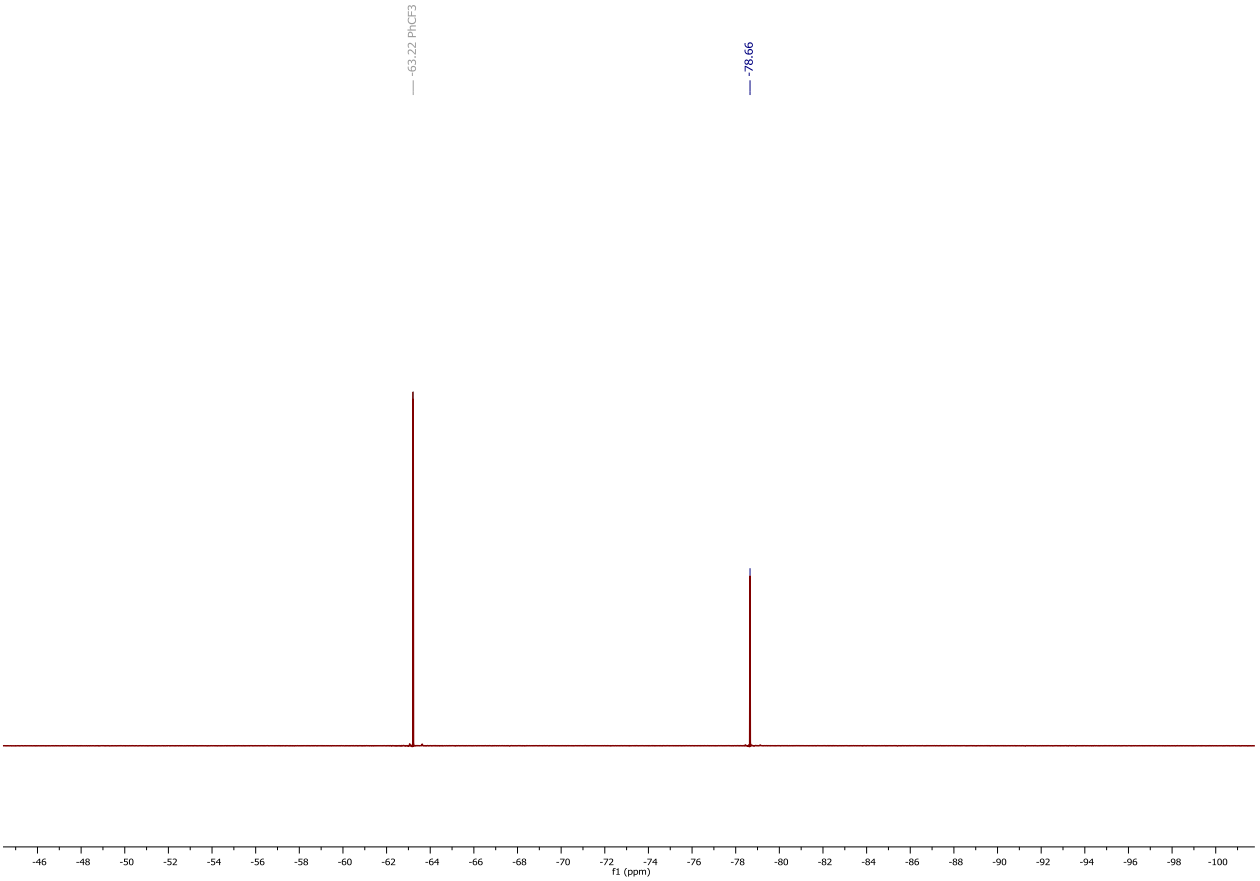

Figure S20: ^{19}F NMR spectrum (471 MHz) of $[Ag_5F(\mathbf{2})_2](OTf)_4$ in acetone-d_6 at 296 K (spectral window from 20 to –220 ppm) showing signal for OTf (signal at –63.2 corresponds to $PhCF_3$).

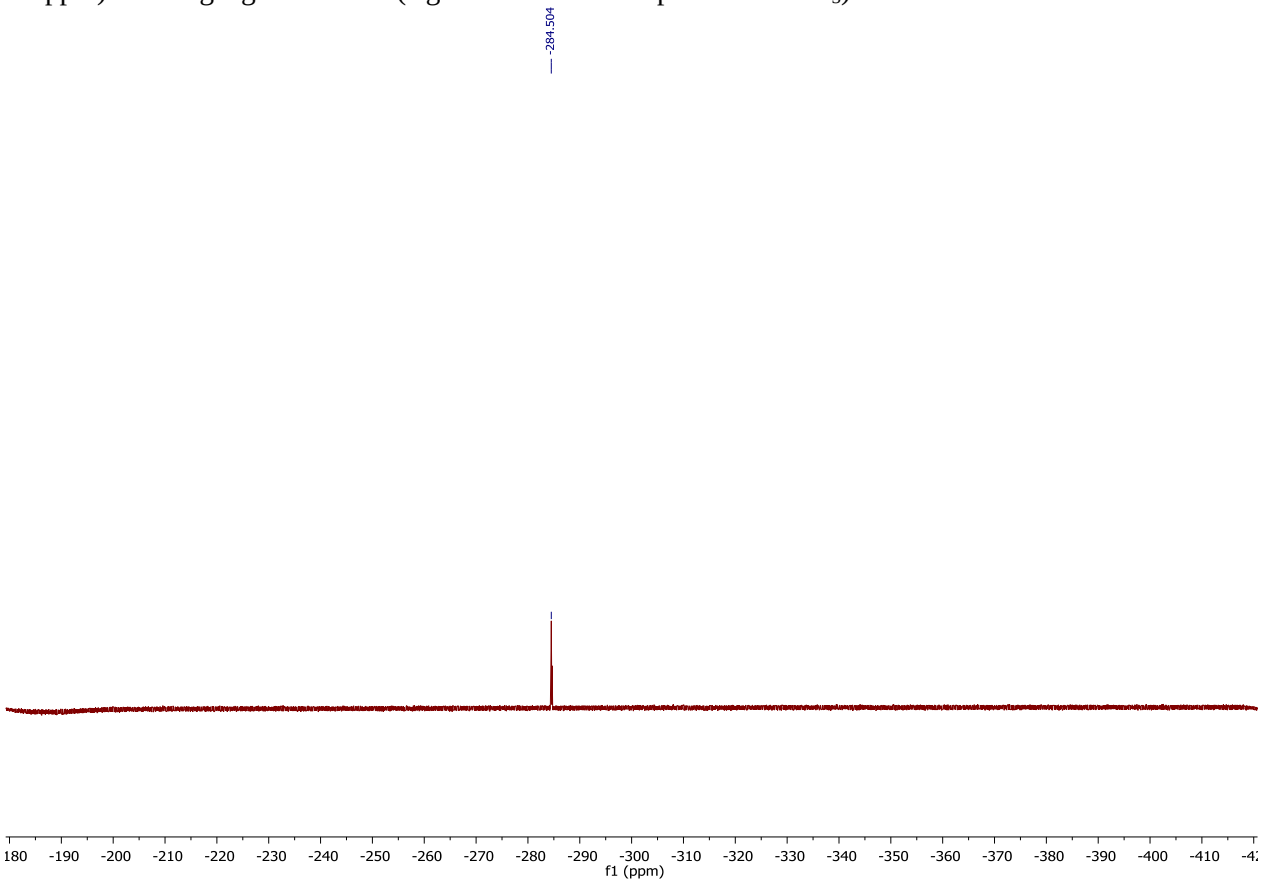

Figure S21: ^{19}F NMR spectrum (471 MHz) of $[Ag_5F(\mathbf{2})_2](OTf)_4$ in acetone-d_6 at 296 K (spectral window from –230 to –470 ppm) showing signal for F^-.

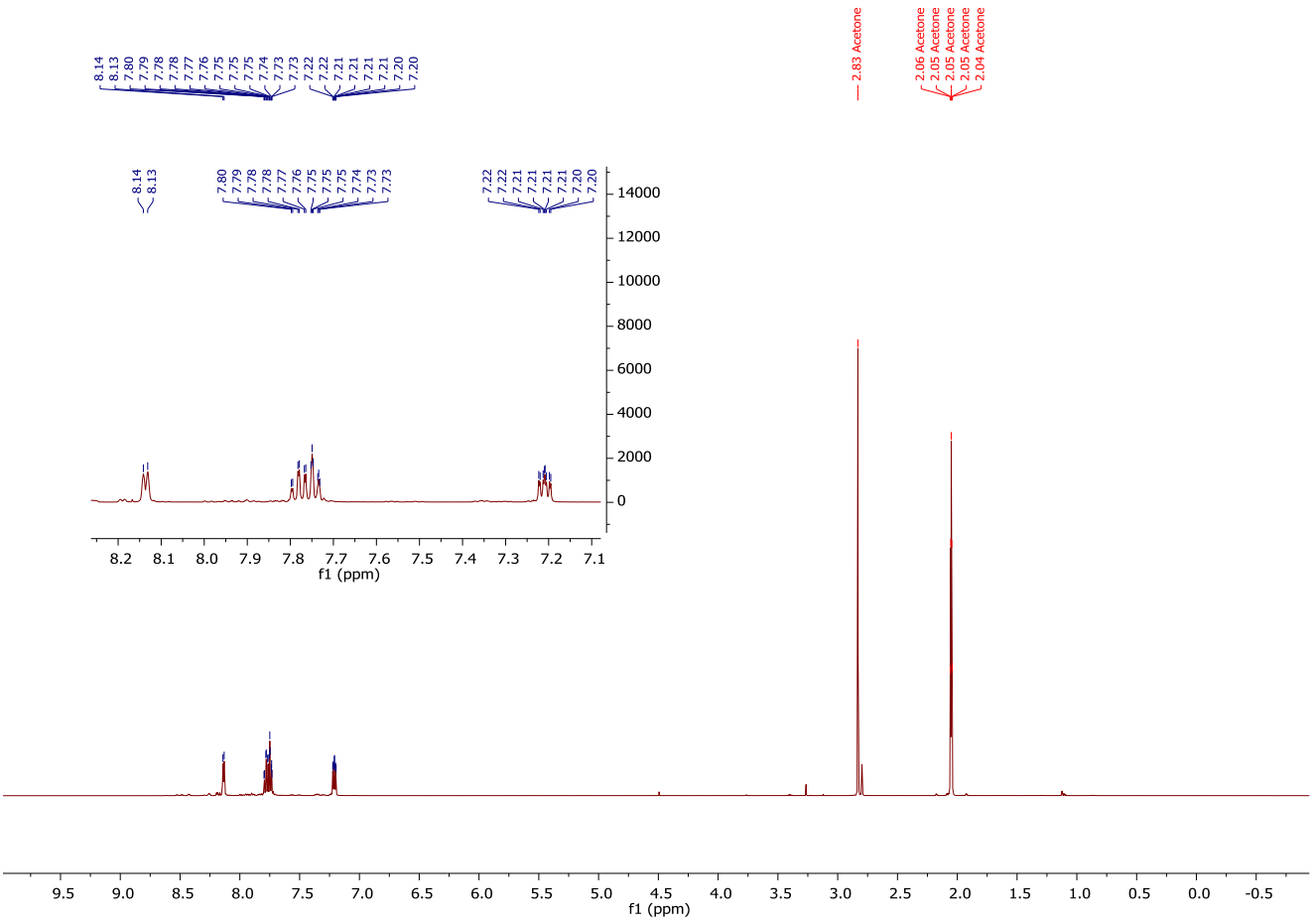

Figure S22: ^{1}H NMR spectrum (500 MHz) of $[Ag_4F(\mathbf{2})_2](PF_6)_3$ in acetone-d_6 at 296 K.

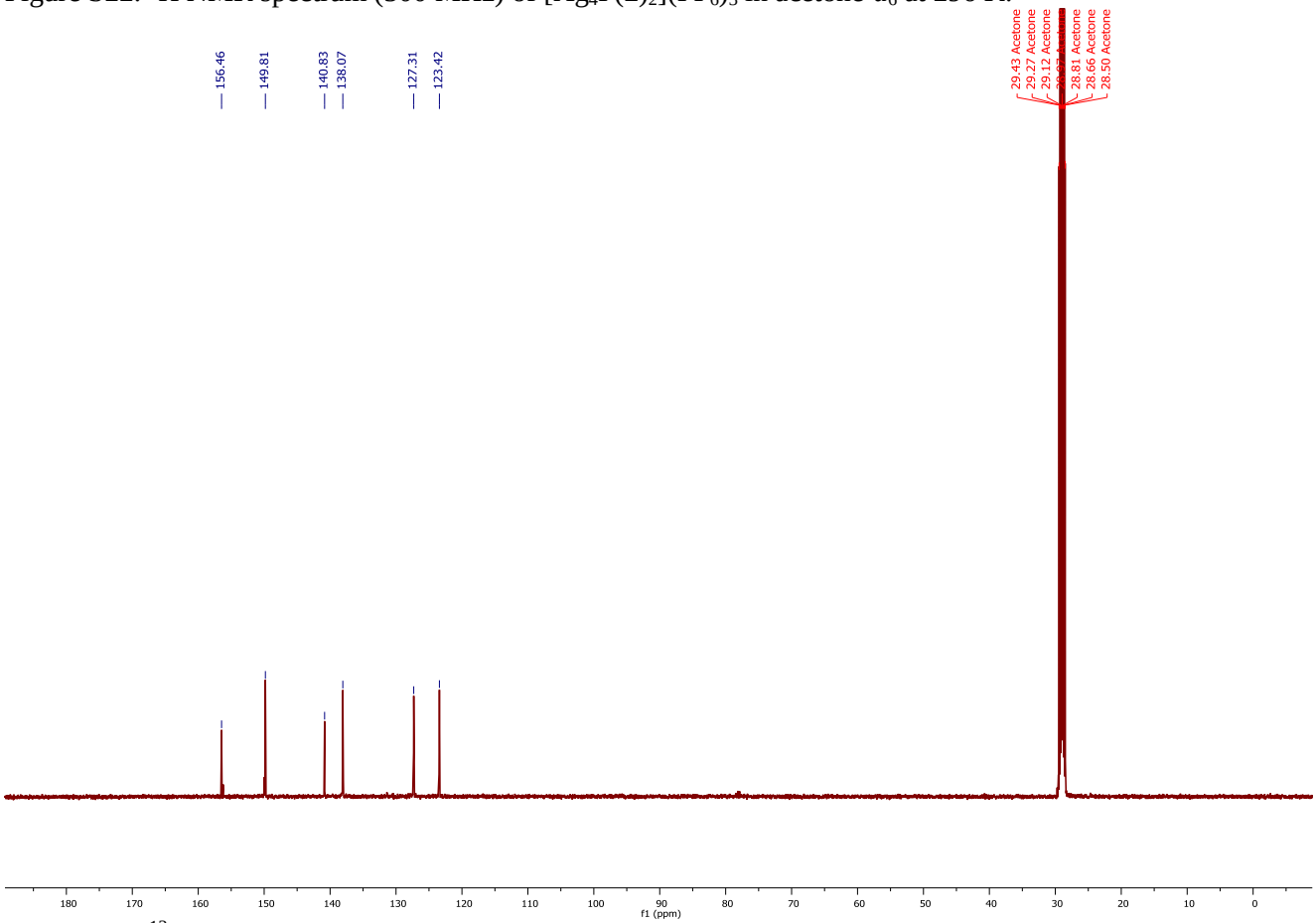

Figure S23: ^{13}C NMR spectrum (126 MHz) of $[Ag_4F(\mathbf{2})_2](PF_6)_3$ in acetone-d_6 at 296 K.

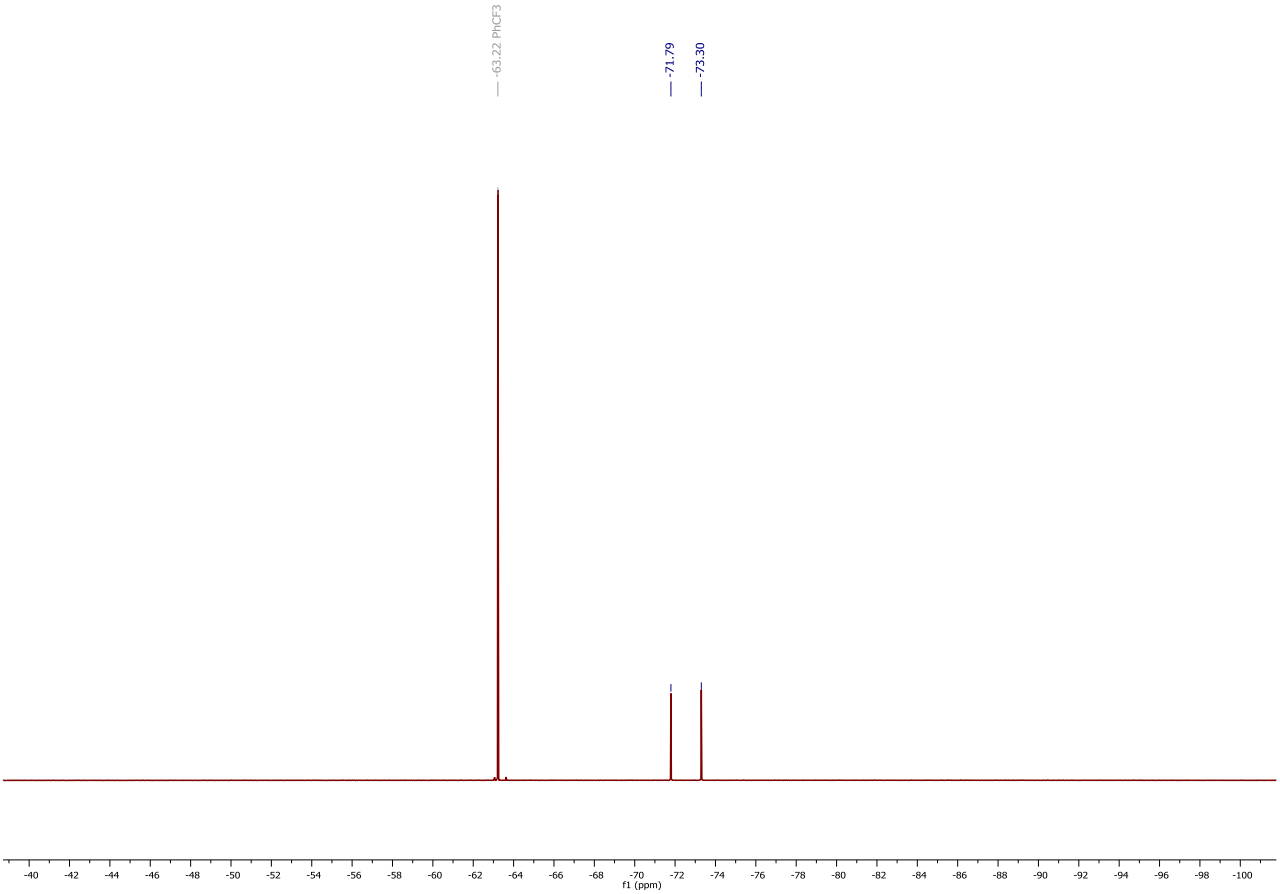

Figure S24: ^{19}F NMR spectrum (471 MHz) of $[Ag_4F(\mathbf{2})_2](PF_6)_3$ in acetone-d_6 at 296 K (spectral window from 20 to –220 ppm) showing signal for PF_6 (d, $^1J_{FP}$ = 708.2 Hz) (signal at –63.2 corresponds to $PhCF_3$).

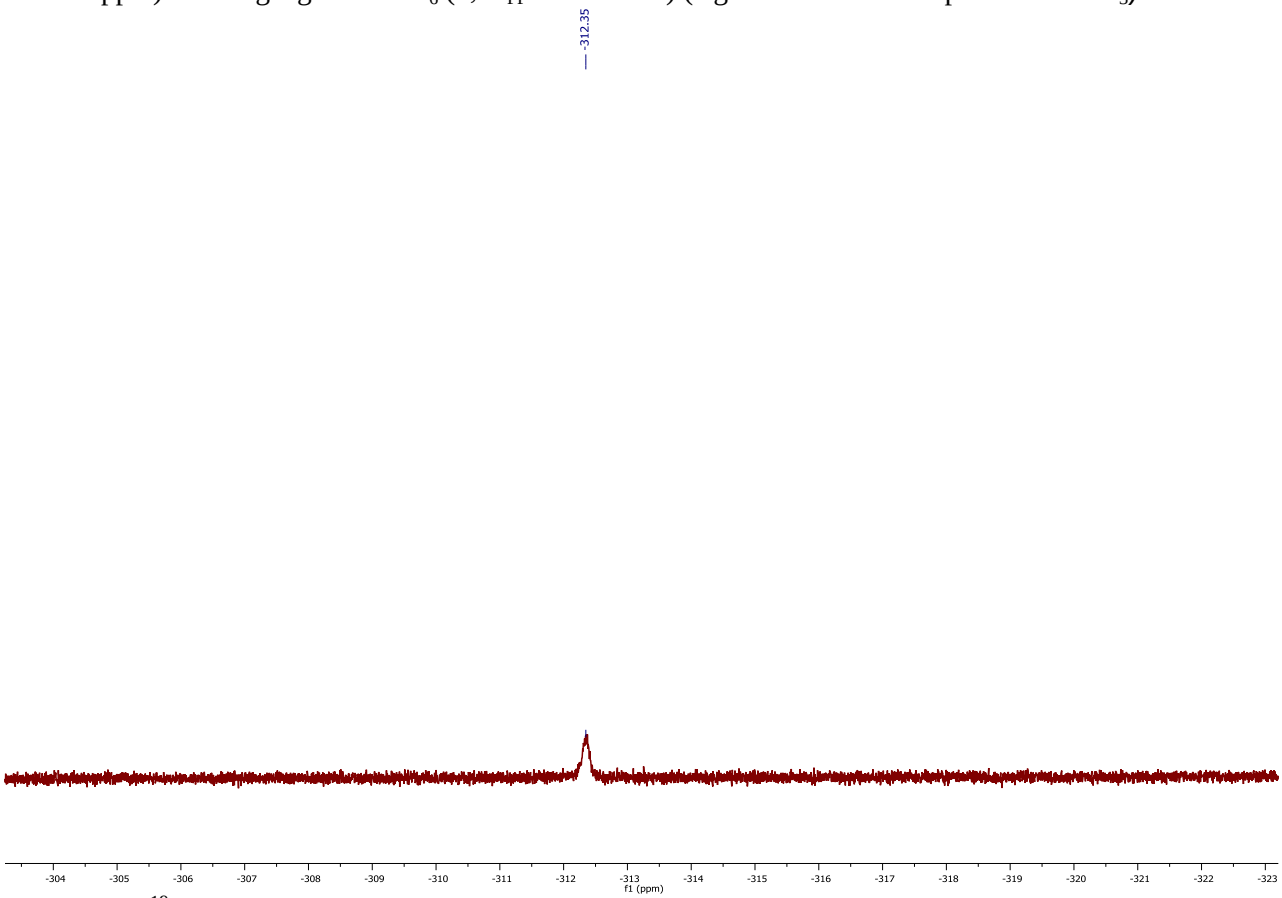

Figure S25: ^{19}F NMR spectrum (471 MHz) of $[Ag_4F(\mathbf{2})_2](PF_6)_3$ in acetone-d_6 at 296 K (spectral window from –230 to –470 ppm) showing signal for F^-.

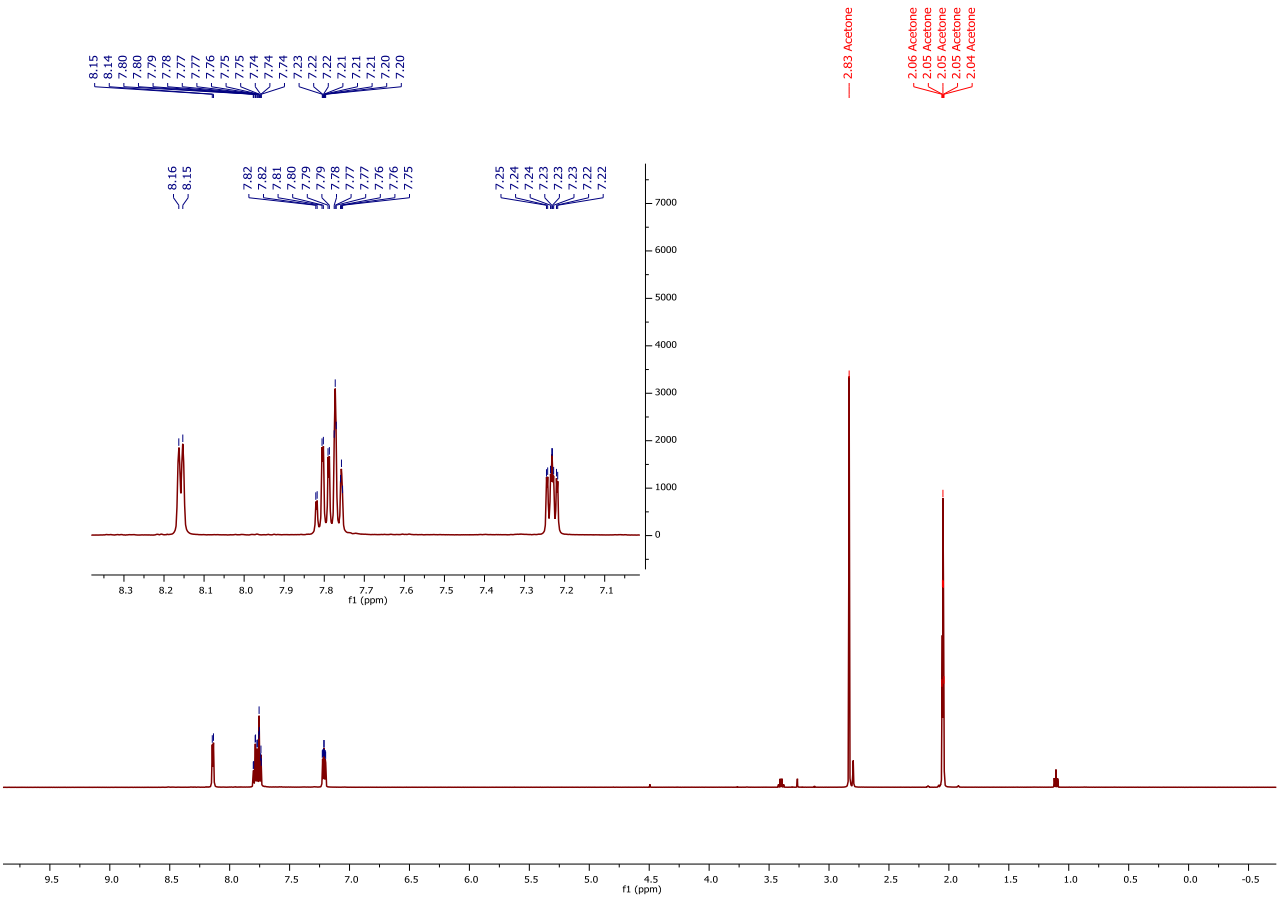

Figure S26: ^{1}H NMR spectrum (500 MHz) of $[Ag_4F(\mathbf{2})_2](SbF_6)_3$ in acetone-d_6 at 296 K.

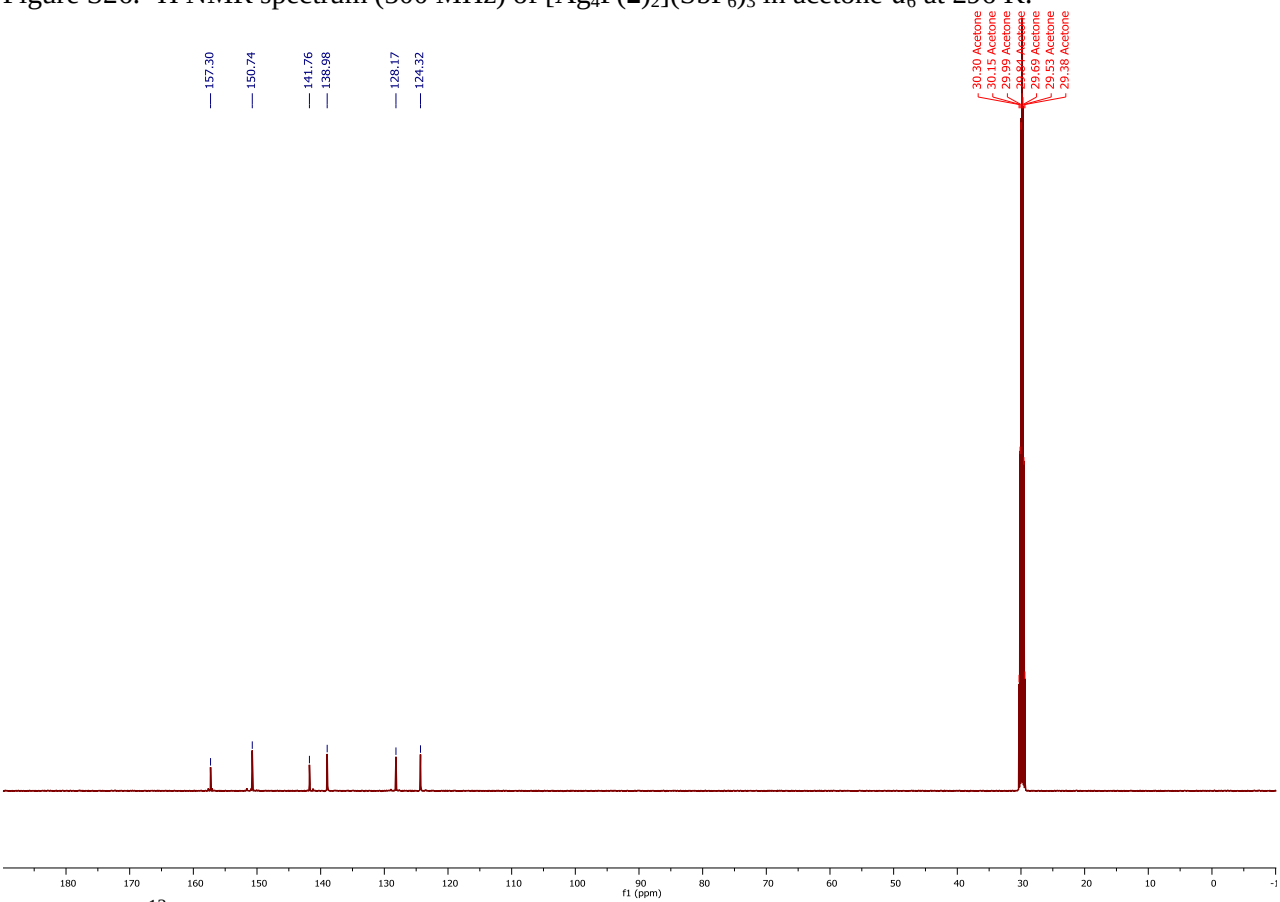

Figure S27: ^{13}C NMR spectrum (126 MHz) of $[Ag_4F(\mathbf{2})_2](SbF_6)_3$ in acetone-d_6 at 296 K.

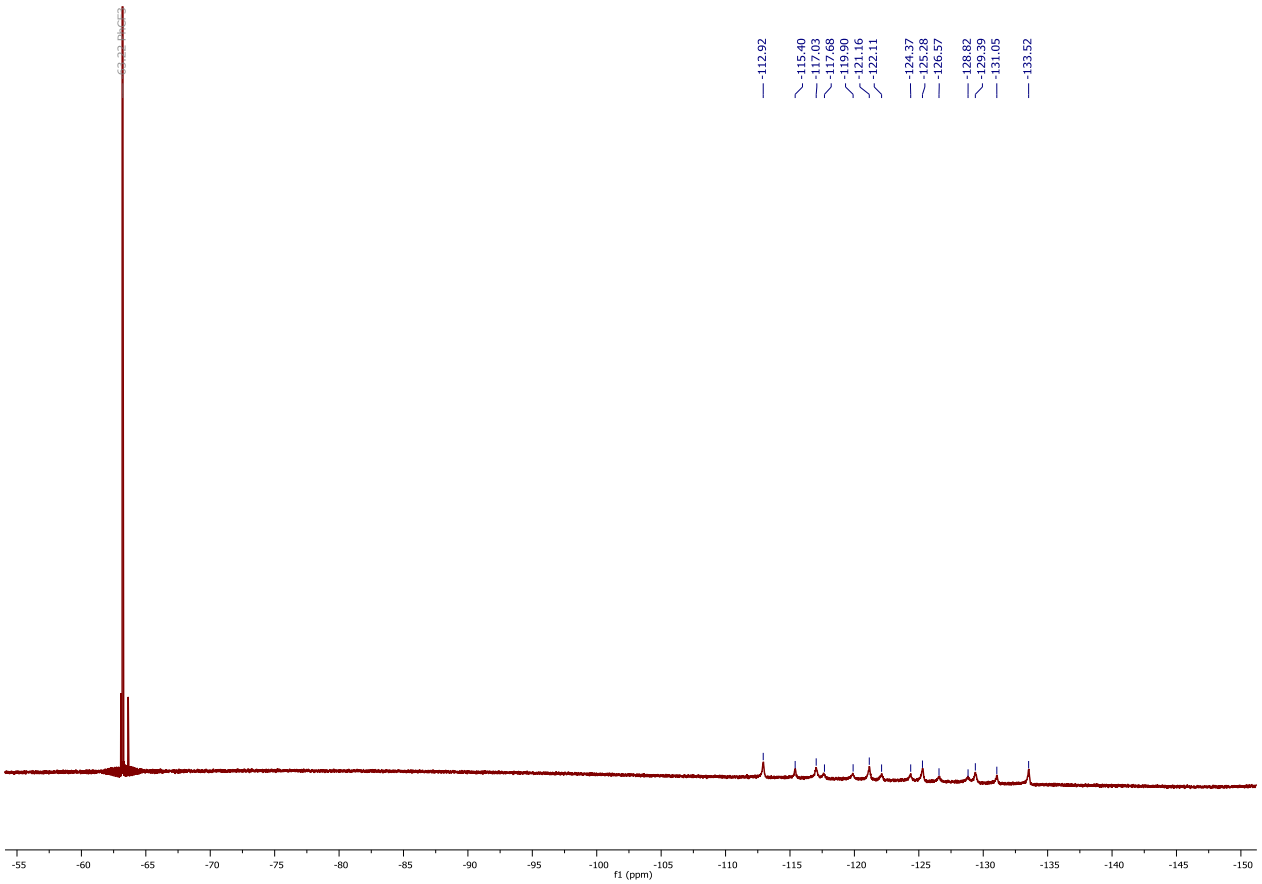

Figure S28: ^{19}F NMR spectrum (471 MHz) of $[Ag_4F(\mathbf{2})_2](SbF_6)_3$ in acetone-d_6 at 296 K (spectral window from 20 to –220 ppm) showing signals for SbF_6 (superposition of a sextet due to $^{121}SbF_6^-$ and an octet due to $^{123}SbF_6^-$, $^1J_F{}^{121}_{Sb}$ = 1941, $^1J_F{}^{123}_{Sb}$ = 1051 Hz) (signal at –63.2 corresponds to $PhCF_3$).

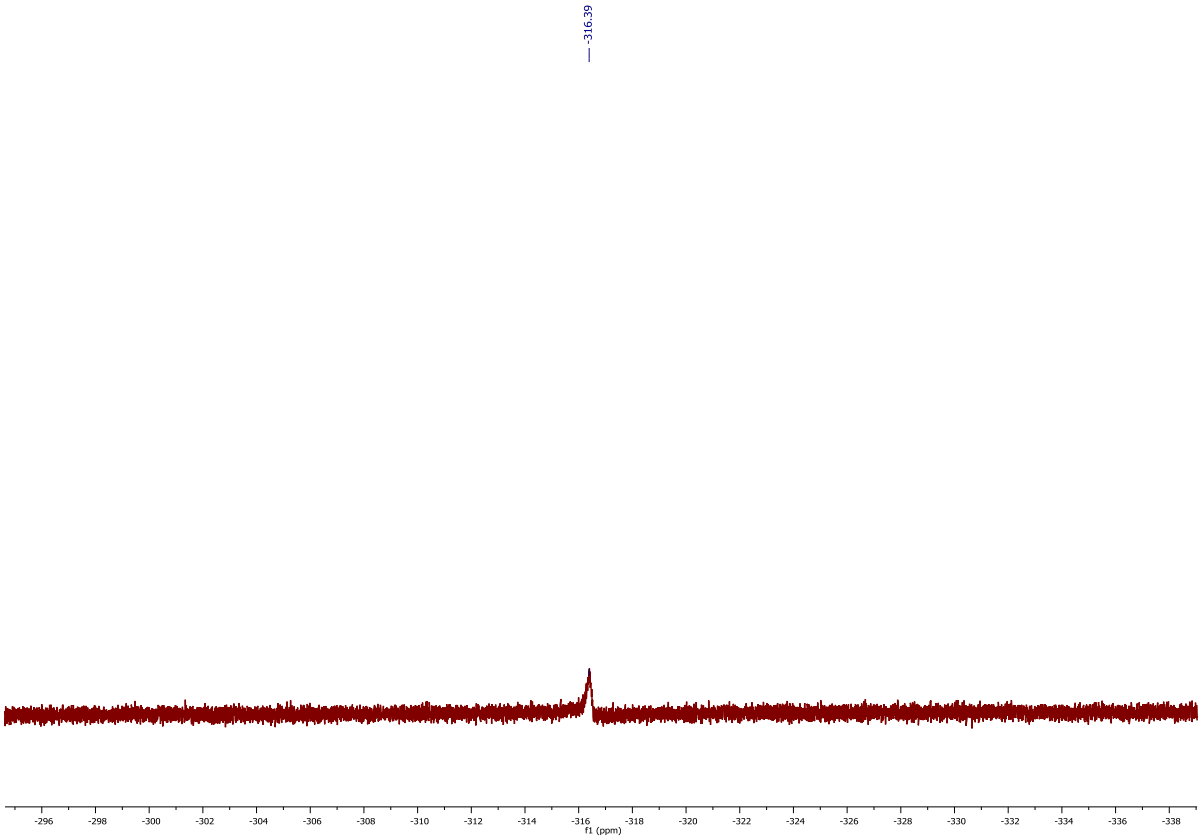

Figure S29: ^{19}F NMR spectrum (471 MHz) of $[Ag_4F(\mathbf{2})_2](SbF_6)_3$ in acetone-d_6 at 296 K (spectral window from –230 to –470 ppm) showing signal for F^-.

Mass spectra

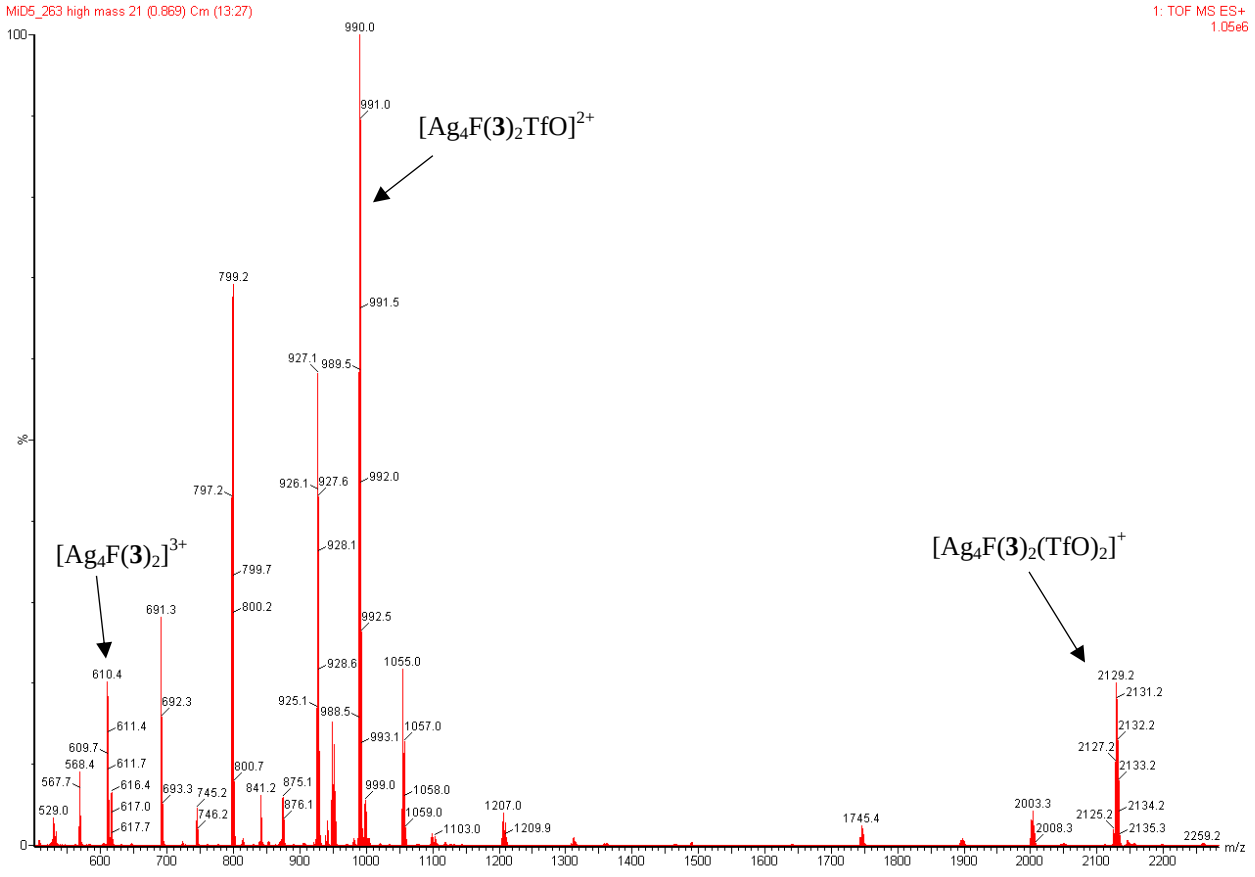

Figure S30: Mass spectrum (TOF-MS) of $[Ag_4F(\mathbf{3})_2](OTf)_3$.

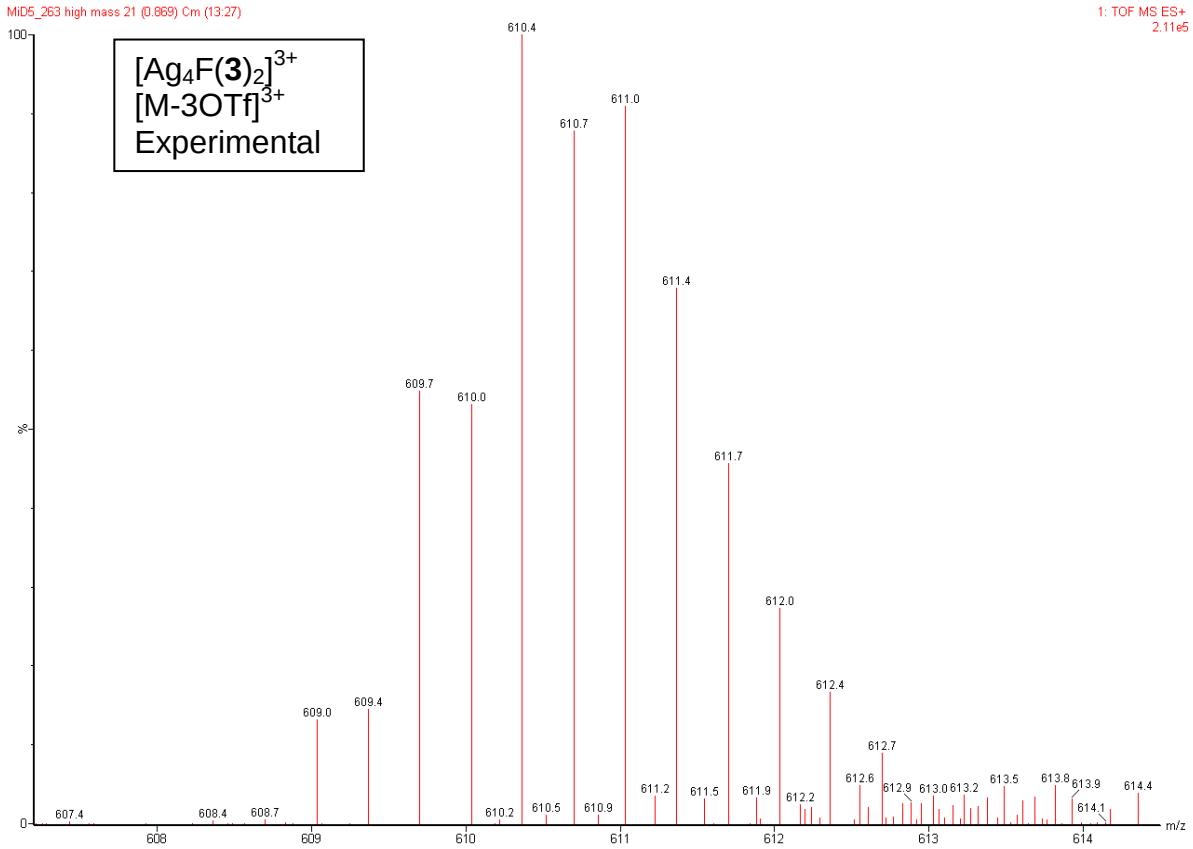

Figure S31: Mass spectrum (TOF-MS) peak corresponding to $[Ag_4F(\mathbf{3})_2]^{3+}$.

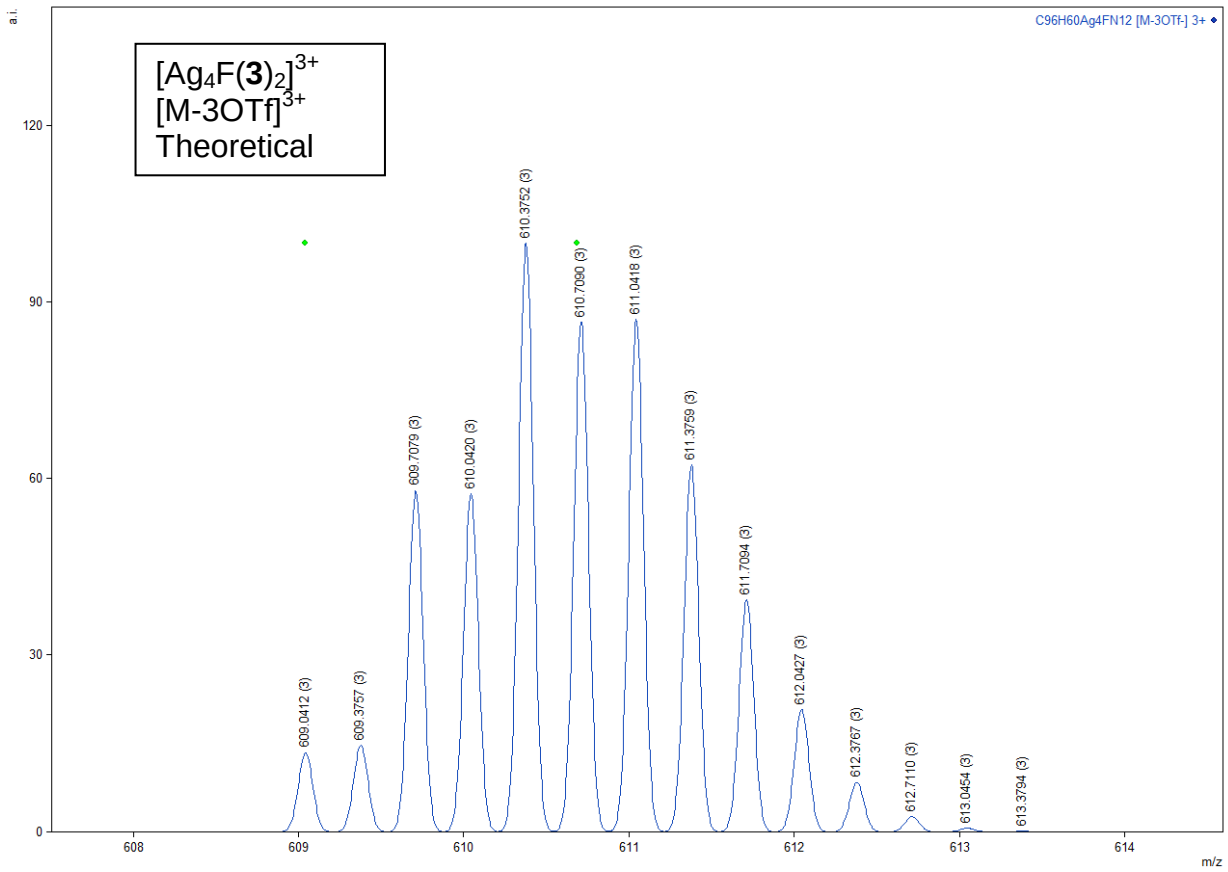

Figure S32: Simulated mass spectrum peak corresponding to $[Ag_4F(\mathbf{3})_2]^{3+}$.

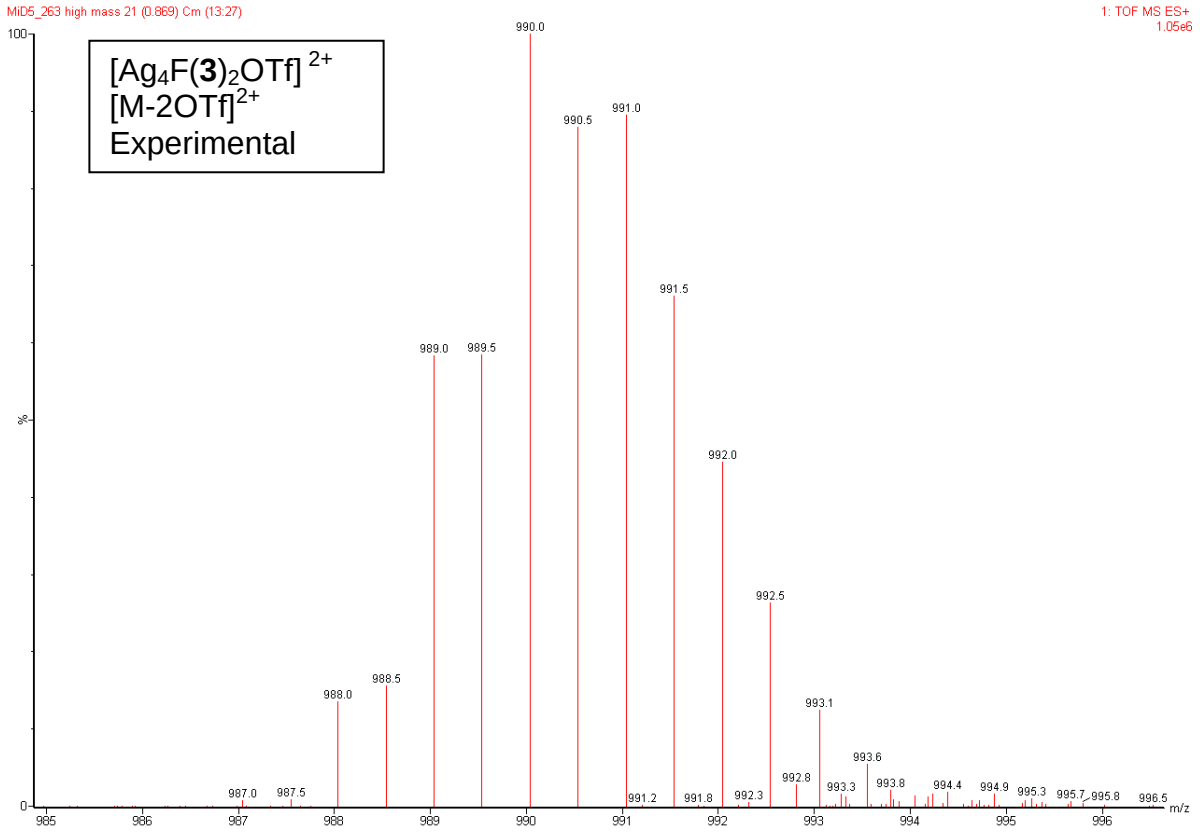

Figure S33: Mass spectrum (TOF-MS) peak corresponding to $[Ag_4F(\mathbf{3})_2OTf]^{2+}$.

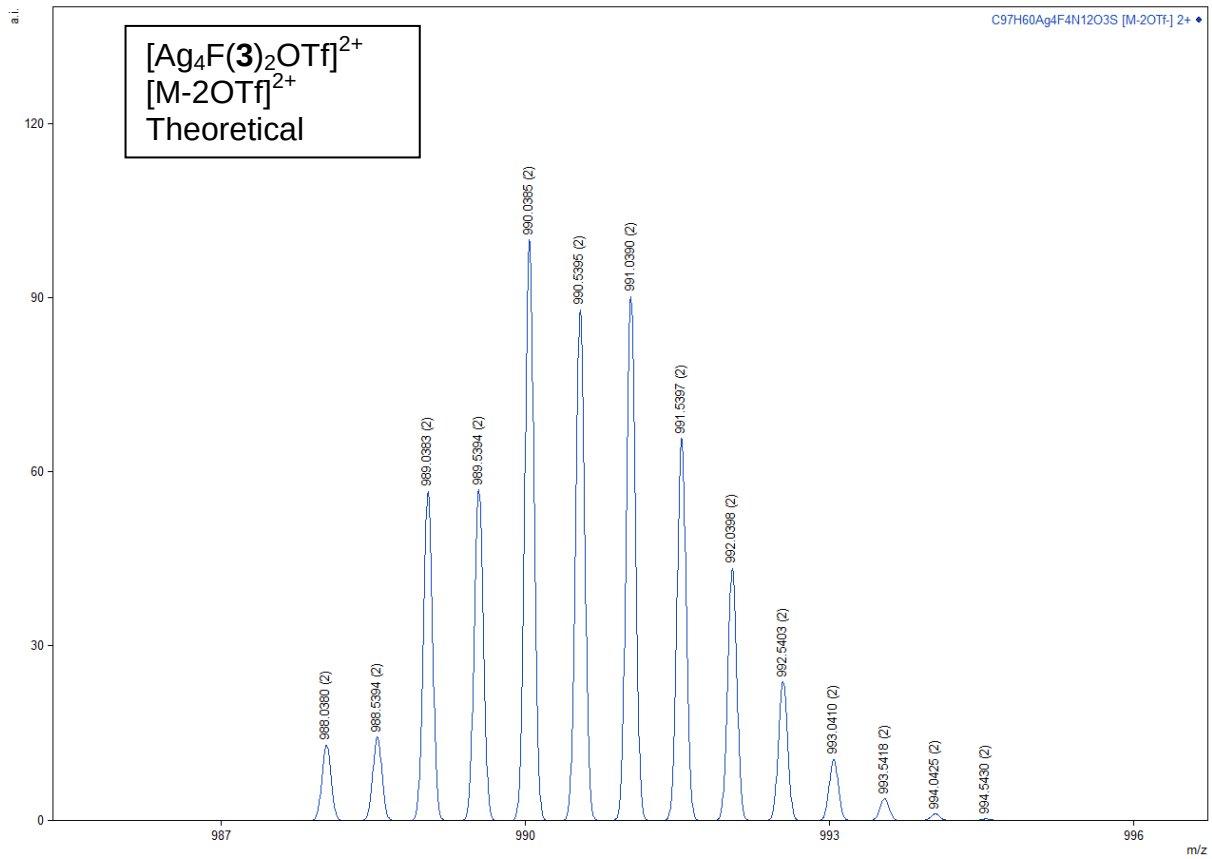

Figure S34: Simulated mass spectrum peak corresponding to $[Ag_4F(\mathbf{3})_2OTf]^{2+}$.

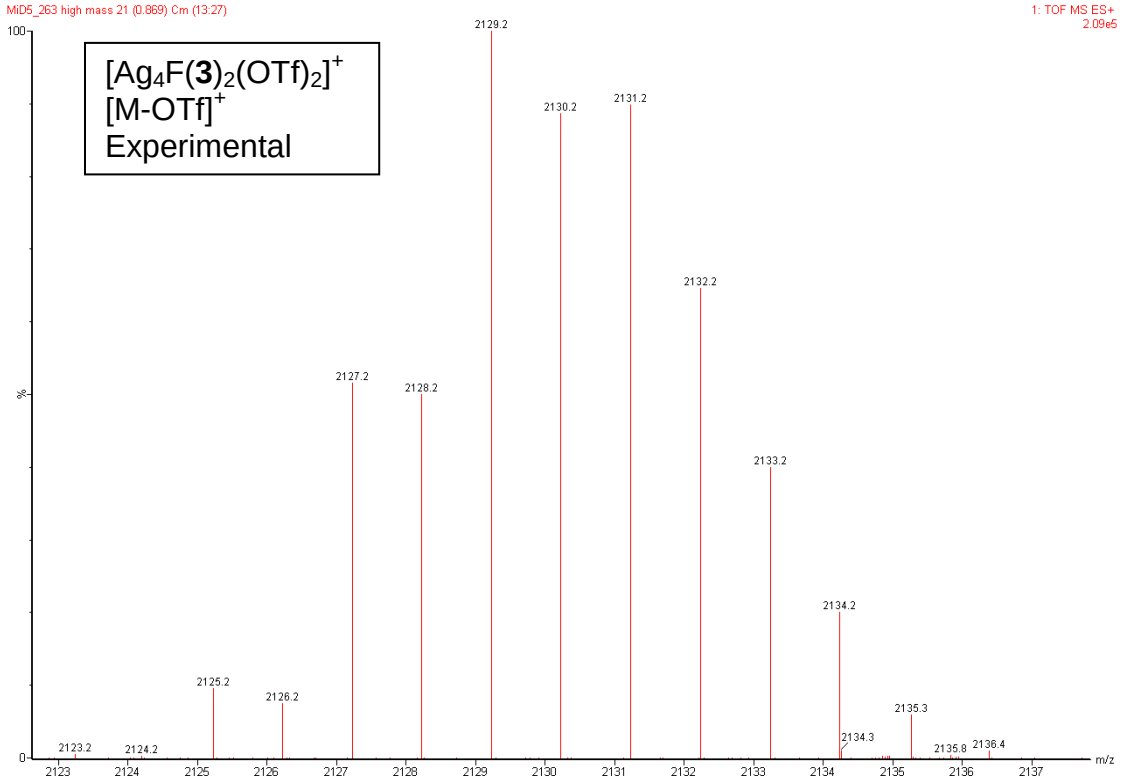

Figure S35: Mass spectrum (TOF-MS) peak corresponding to $[Ag_4F(\mathbf{3})_2(OTf)_2]^+$.

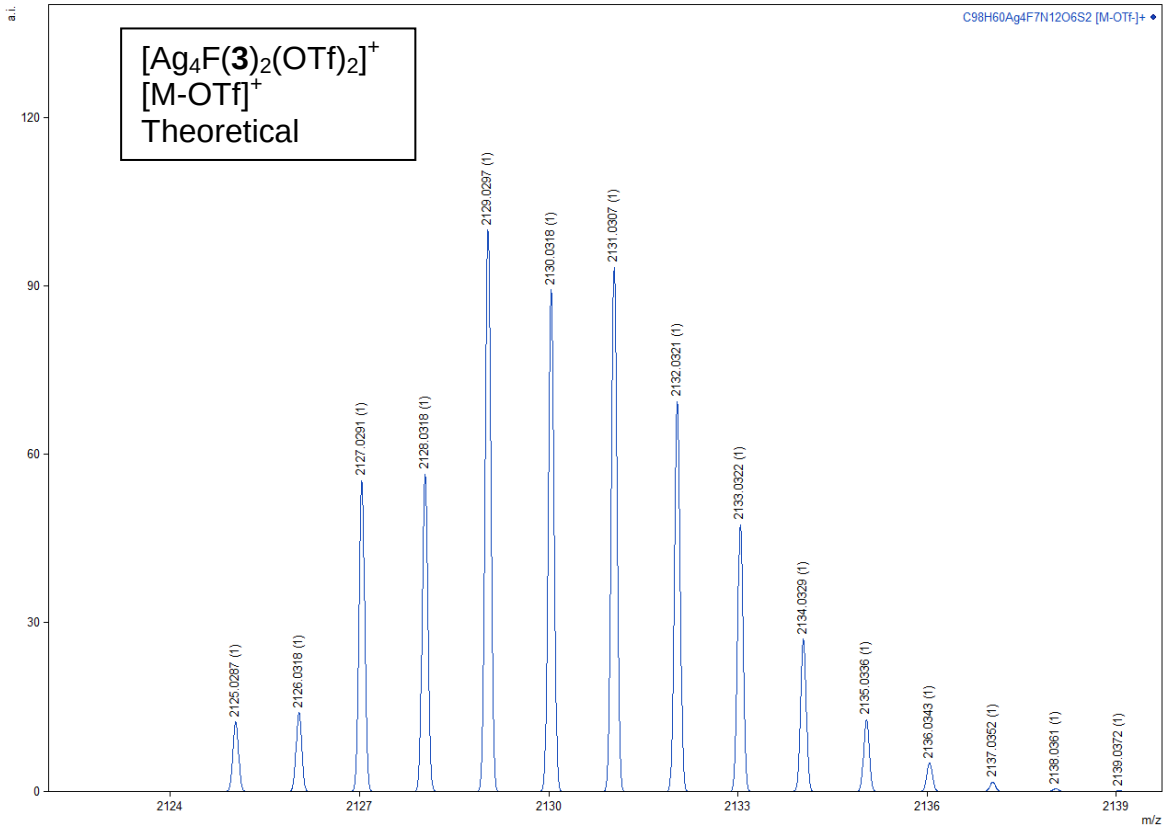

Figure S36: Simulated mass spectrum peak corresponding to $[Ag_4F(\mathbf{3})_2(OTf)_2]^+$.

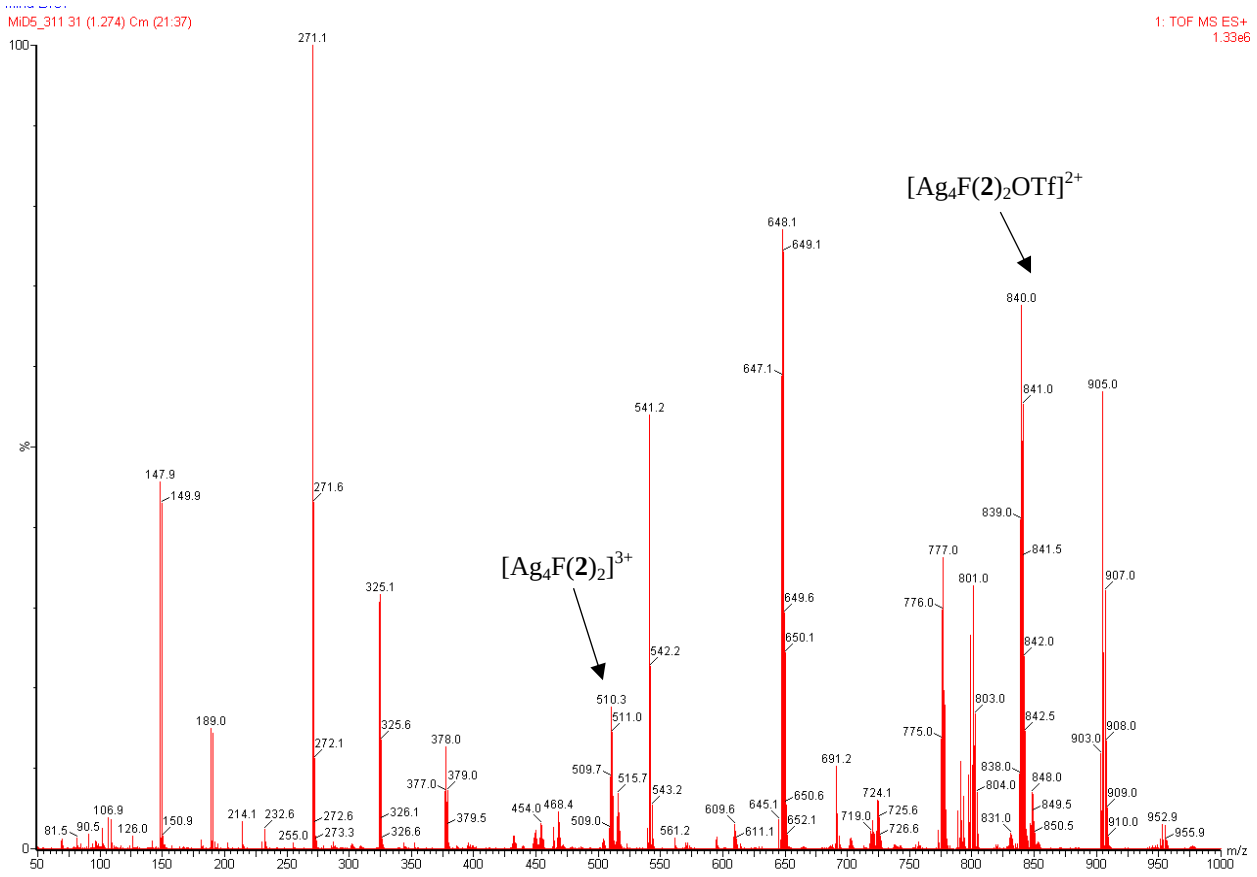

Figure S37: Mass spectrum (TOF-MS) of $[Ag_5F(\mathbf{2})_2](OTf)_4$.

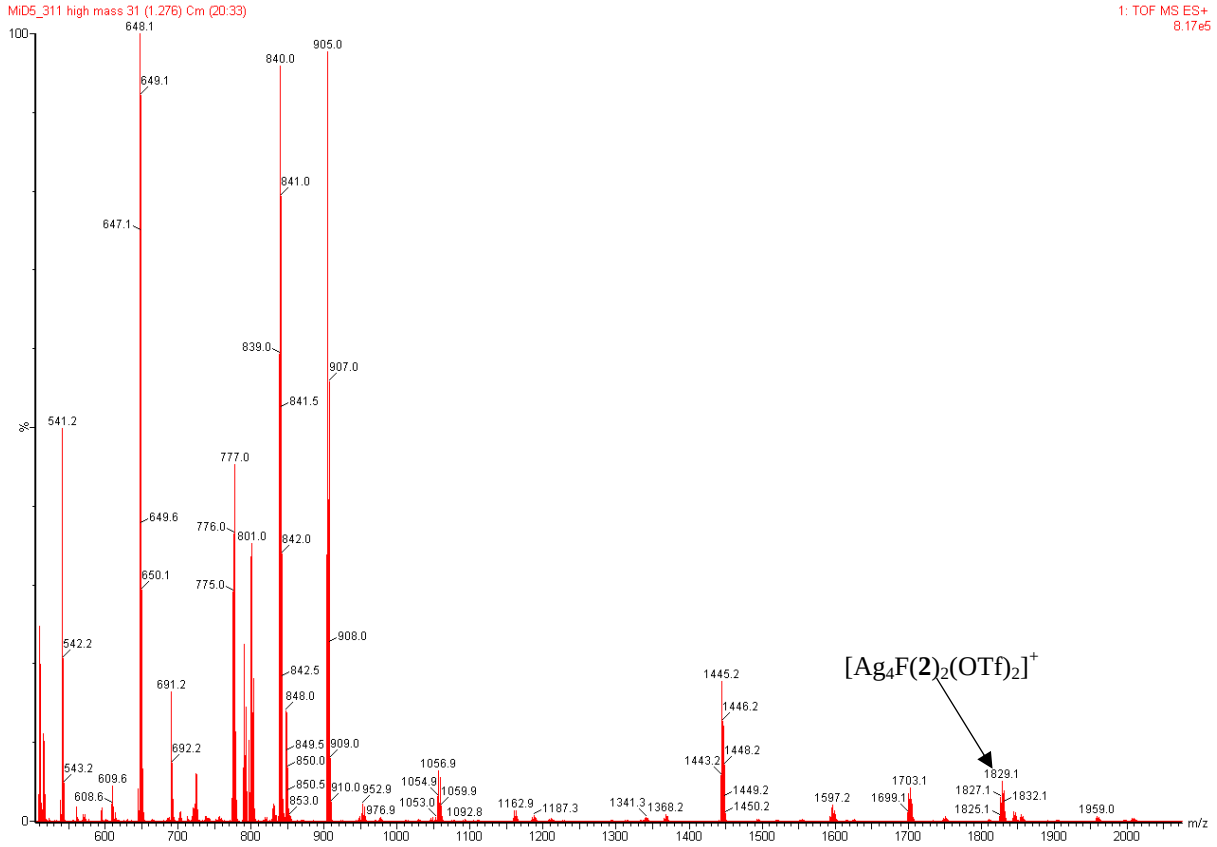

Figure S38: Mass spectrum (TOF-MS) of $[Ag_5F(\mathbf{2})_2](OTf)_4$.

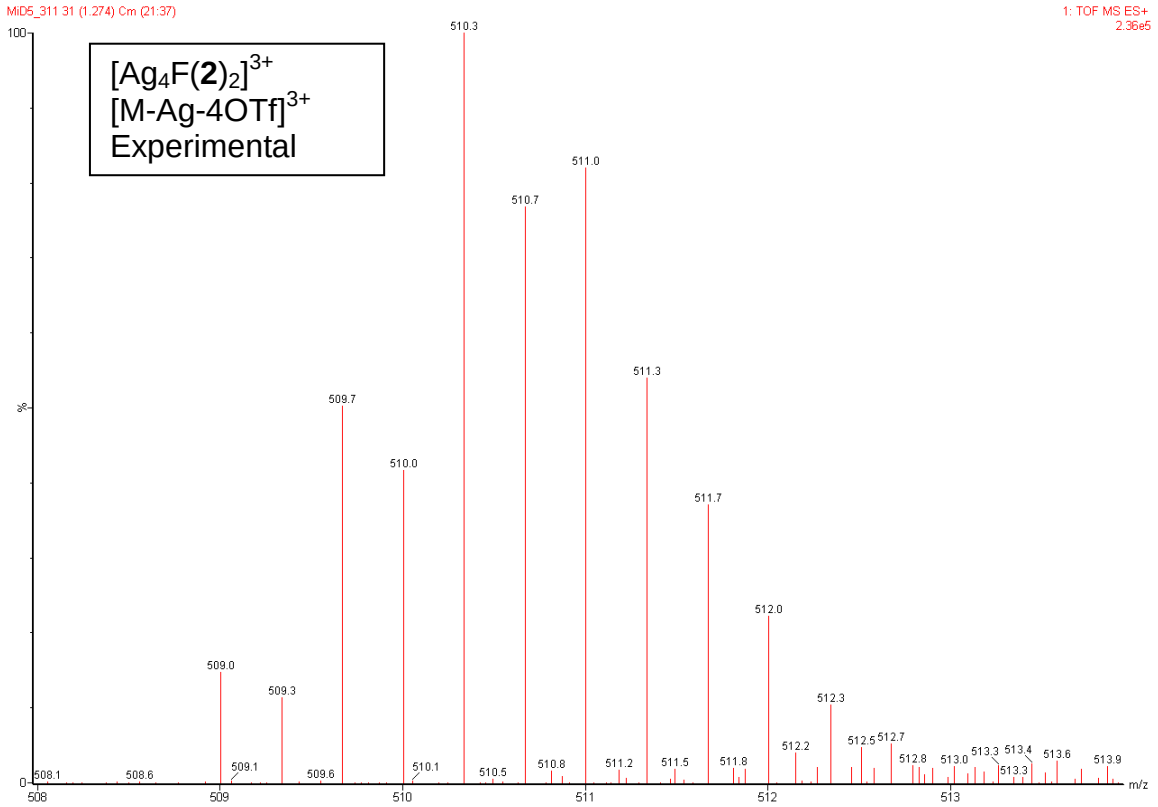

Figure S39: Mass spectrum (TOF-MS) peak corresponding to $[Ag_4F(\mathbf{2})_2]^{3+}$ arising from $[Ag_5F(\mathbf{2})_2]^{4+}$ after dissociation of one Ag(I) ion.

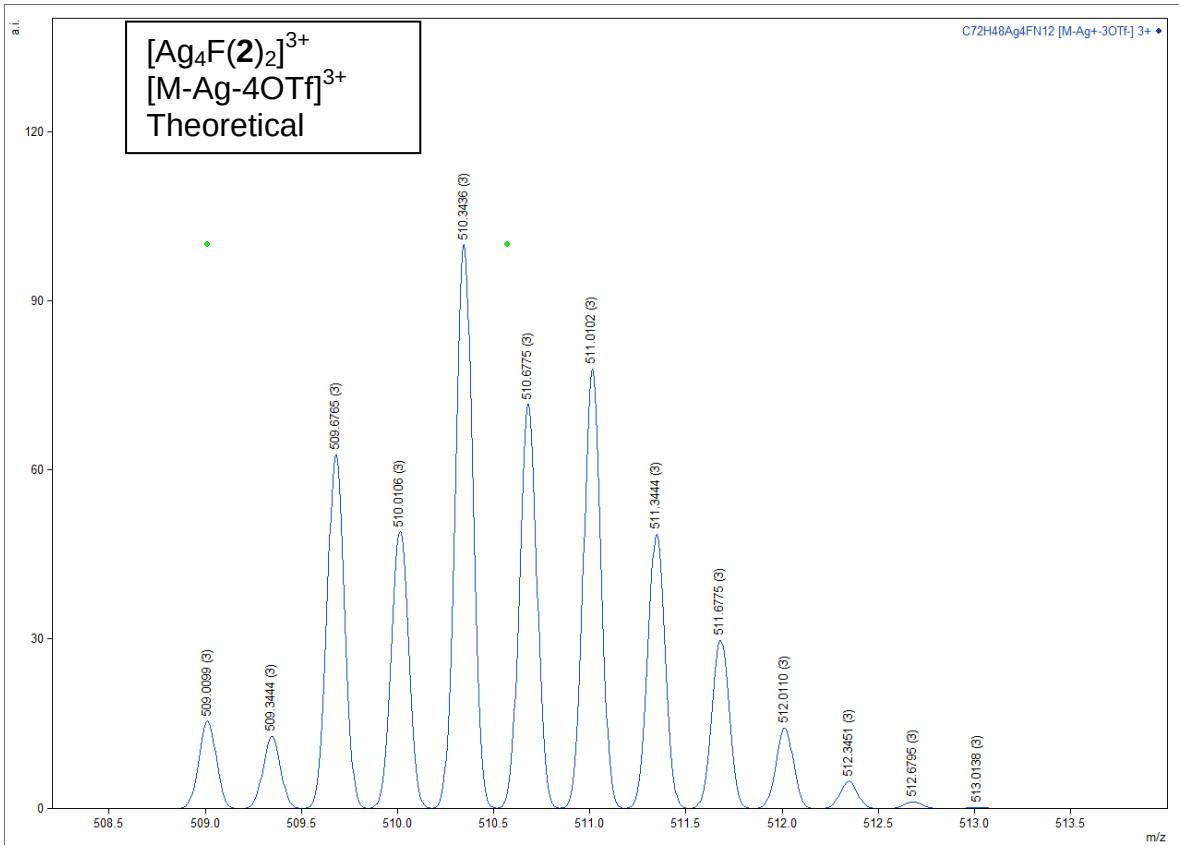

Figure S40: Simulated mass spectrum peak of $[Ag_4F(\mathbf{2})_2]^{3+}$

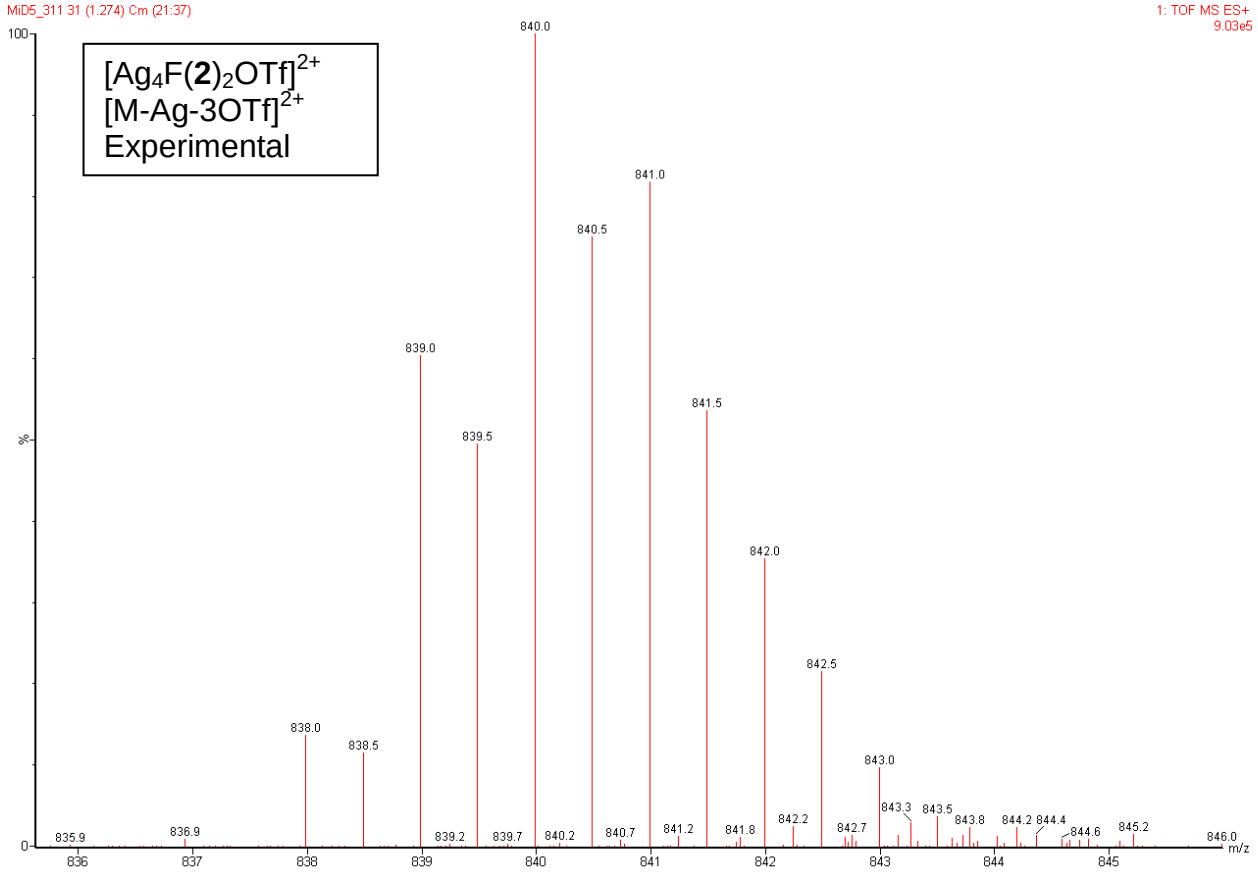

Figure S41: Mass spectrum (TOF-MS) peak corresponding to $[Ag_4F(\mathbf{2})_2OTf]^{2+}$ arising from $[Ag_5F(\mathbf{2})_2OTf]^{3+}$ after dissociation of one Ag(I) ion.

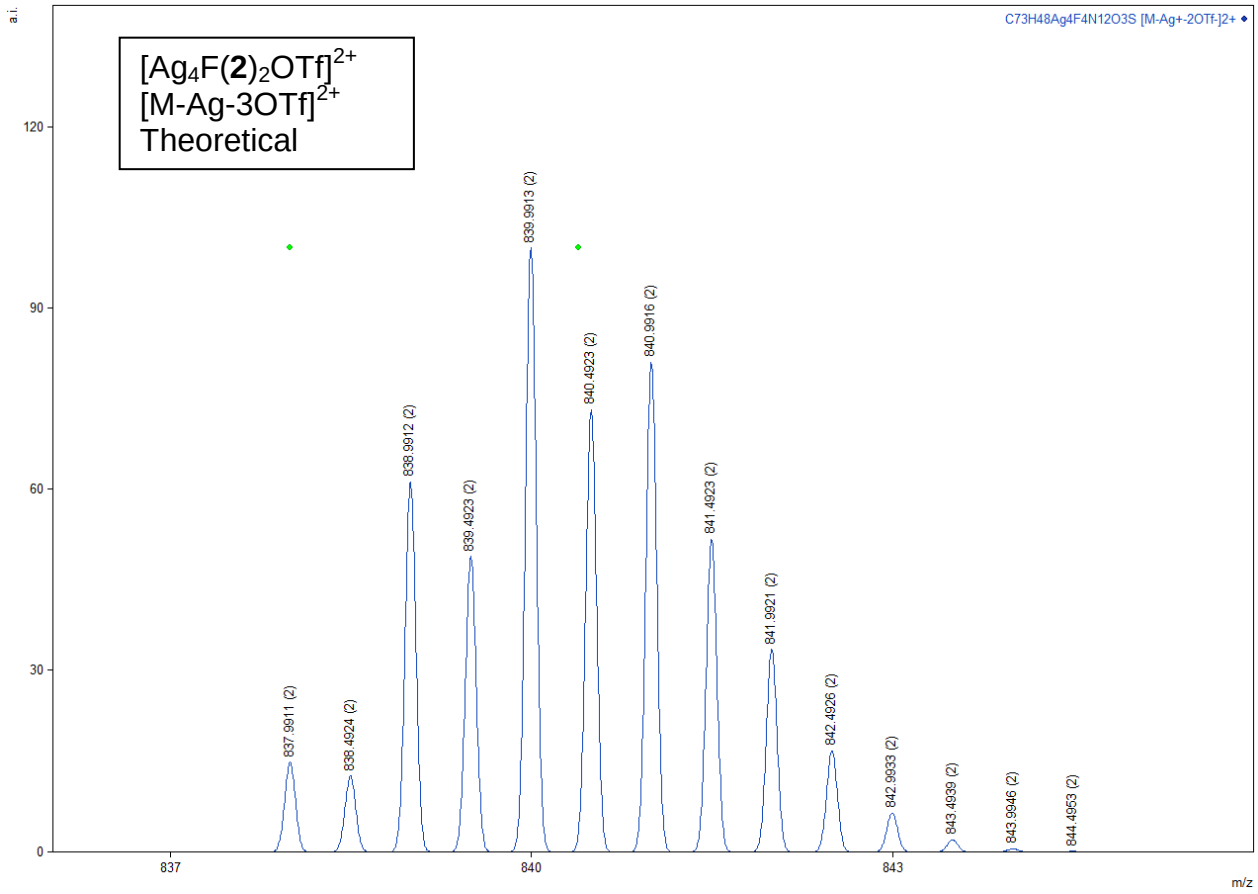

Figure S42: Simulated mass spectrum peak of $[Ag_4F(2)_2OTf]^{2+}$.

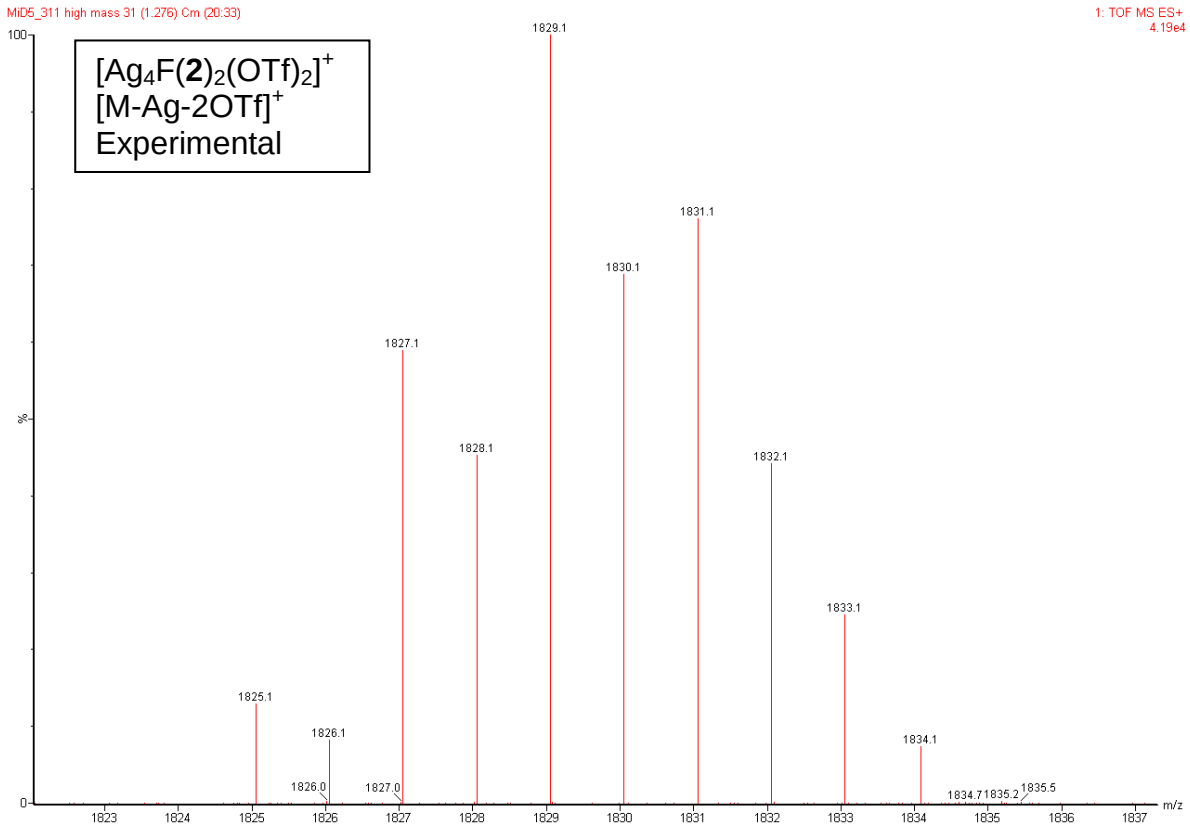

Figure S43: Mass spectrum (TOF-MS) peak corresponding to $[Ag_4F(\mathbf{2})_2(OTf)_2]^+$ arising from $[Ag_5F(\mathbf{2})_2(OTf)_2]^{2+}$ after dissociation of one Ag(I) ion.

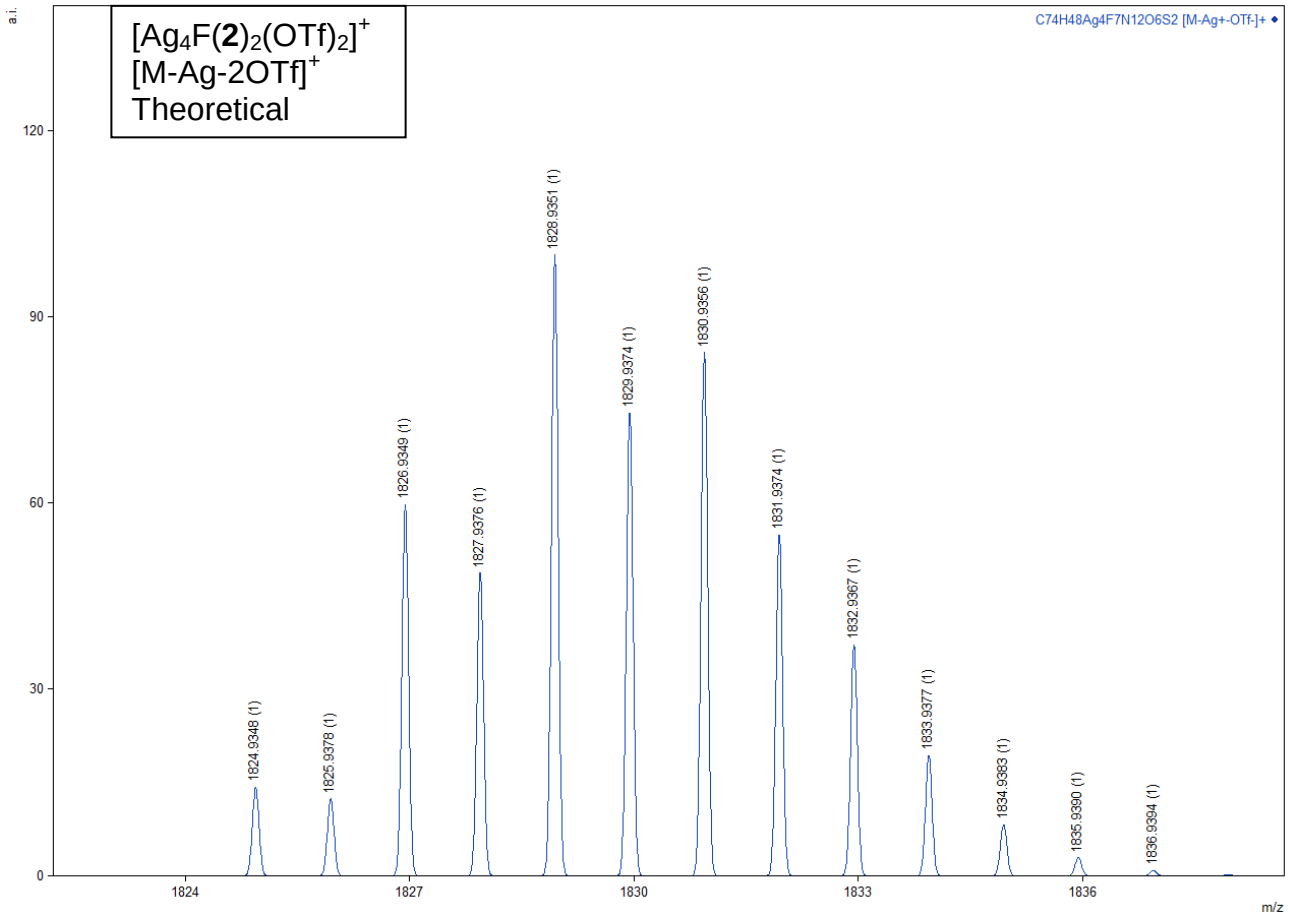

Figure S44: Simulated mass spectrum peak of $[Ag_4F(\mathbf{2})_2(OTf)_2]^+$.

X-ray Crystallographic studies

Crystal data for complexes $[Ag_4F(\mathbf{2})_2](OTf)_3$, $[Ag_4F(\mathbf{3})_2](OTf)_3{\cdot}3H_2O$ and $[Ag_5F(\mathbf{2})_2](OTf)_4{\cdot}2H_2O{\cdot}C_3H_6O{\cdot}C_6H_6$ were collected at 150 K on an Agilent Technologies SuperNova Dual diffractometer using monochromated Mo-*K*α radiation (λ = 0.71073 Å). The data were processed using CrysAlis Pro [3]. Structures were solved with the ShelXT [4] structure solution program using intrinsic phasing and refined by a full-matrix least-squares procedure based on F^2 with ShelXL [5] implemented in the Olex^2 program suite [6]. All non-hydrogen atoms were readily located and refined anisotropically unless otherwise noted. Hydrogen atoms were initially located in the difference Fourier maps and were subsequently included in the model at geometrically calculated positions and refined by using a riding model unless otherwise noted. For $[Ag_4F(\mathbf{2})_2](OTf)_3$ the complex cation was readily located and refined, however, only few atoms of the counterions were located having very large anisotropic displacement parameters and were in further steps of the refinement removed from the model. The scattering contributions of the disordered counterions were removed with a solvent mask procedure implemented in Olex^2. The counterion contribution was not included in the reported molecular weight and density. Although the crystals were of low quality (R_{int} = 0.1833) the data were of sufficient quality to determine the structure of the complex cation. In the structure of $[Ag_4F(\mathbf{3})_2](OTf)_3{\cdot}3H_2O$ hydrogen atoms on water oxygen atoms were not found in difference Fourier maps and were not included in the refinement. One water molecule and one triflate anion were disordered over a 2-fold rotation axis in the fixed ratio 0.50/0.50. Water molecules O8–O10 were refined with a fixed occupancy of 0.33 and restrained U^{ij} components. Hydrogen atoms attached to water molecules O1 and O8–O10 were not found in Fourier difference maps and were not included in the model. Crystals of $[Ag_5F(\mathbf{2})_2](OTf)_4{\cdot}2H_2O{\cdot}C_3H_6O{\cdot}C_6H_6$ were obtained by recrystallization from an acetone/benzene/ethyl acetate mixture and the crystal structure contains electron density that belongs to disordered solvate molecules. One triflate anion was refined by fixing the coordinates of C76 and O11, and restraining U^{ij} components for O11, C76, F12 and F13. Benzene solvate molecule atoms C80–C85 were refined isotropically, and hydrogen atoms were not included in the model. Water molecules O14 and O16 were refined with a fixed occupancy ratio of 0.50 and restrained U^{ij} components. Hydrogen atoms attached to water molecules O14–O16 were not found in Fourier difference maps and were not included in the model. The scattering contributions of the disordered solvate molecules, including the unrecognized C_4O_2 fragment were removed with a solvent mask procedure implemented in Olex^2. The unmodeled solvent contribution was not included in the reported molecular weight and density. Although the crystals were of low quality and the wR_2 value is 0.4596, the data were of sufficient quality to determine the molecular and crystal structure. Details of the crystal, data collection and refinement parameters as well as selected bond distances and angles are given in Tables S1–S4. CCDC 1971156–1971158 contains the supplementary crystallographic data for this article.

Table S1: Crystal data and structure refinement.

Formula	$[Ag_4F(\mathbf{2})_2](OTf)_3$	$[Ag_4F(\mathbf{3})_2](OTf)_3{\cdot}3H_2O$	$[Ag_5F(\mathbf{2})_2](OTf)_4{\cdot}2H_2O{\cdot}C_3H_6O{\cdot}C_6H_6$
Formula	$C_{72}H_{48}Ag_4FN_{12}$	$C_{99}H_{66}Ag_4F_{10}N_{12}O_{12}S_3$	$C_{86}H_{64}Ag_5F_{13}N_{12}O_{15}S_4$
M_r	1531.70	2333.29	2420.08
T (K)	150.00(10)	150.00(10)	150.00(10)
Crystal system	Orthorhombic	Trigonal	Monoclinic
Space group	*Pnnn*	$P3_221$	$P2_1/n$
a (Å)	12.0033(11)	21.0986(6)	16.2257(4)
b (Å)	16.0675(7)	21.0986(6)	27.2171(7)
c (Å)	19.9815(12)	19.5901(5)	22.3456(5)
α (°)	90	90	90
β (°)	90	90	90.166(2)
γ (°)	90	120	90
Volume (Å^3)	3853.7(4)	7552.2(5)	9868.1(4)
Z	2	3	4
D_c (g/cm^3)	1.320	1.539	1.629
μ (mm^{-1})	1.048	0.912	1.149
F(000)	1522.0	3498.0	4800.0
Reflections collected	42203	26760	88317
Independent reflections (R_{int})	5416 (0.1833)	11483 (0.0250)	22582 (0.0732)
Data/restraints/parameters	5416/0/202	11483/18/682	22582/36/1182
R, wR_2 [$I > 2\sigma(I)$][a]	0.1339, 0.3931	0.0392, 0.1018	0.1609, 0.4596
R, wR_2 (all data)[a]	0.1919, 0.4347	0.0489, 0.1109	0.1779, 0.4742
GOF, S[b]	1.234	1.023	1.908
Largest diff. peak/hole / e Å^{-3}	2.06/–1.78	0.96/–0.60	2.09/–2.48
Flack parameter	/	–0.028(8)	/

[a] $R = \sum||F_o| - |F_c||/\sum|F_o|$, $wR_2 = \{\sum[w(F_o^2 - F_c^2)^2]/\sum[w(F_o^2)^2]\}^{1/2}$. [b] $S = \{\sum[(F_o^2 - F_c^2)^2]/(n/p)\}^{1/2}$, where n is the number of reflections and p is the total number of parameters refined.

Table S2: Selected bond distances (Å) and angles (°) for $[Ag_4F(\mathbf{2})_2](OTf)_3$.

Distance (Å)			
Ag1–F1	2.3204(8)	Ag1–N3^{iii}	2.392(7)
Ag1–N1	2.427(8)	Ag1···Ag1^{i}	3.366(2)
Ag1–N2^{i}	2.216(6)	Ag1···Ag1^{ii}	3.195(2)
Angle (°)			
F1–Ag1–N1	105.59(17)	N3^{iii}–Ag1–N1	81.6(3)
F1–Ag1–N3^{iii}	106.96(18)	Ag1–F1–Ag1^{iii}	179.33(3)
N2^{ii} –Ag1–F1	121.1(2)	Ag1–F1–Ag1^{ii}	93.00(6)
N2^{ii}–Ag1–N1	116.2(3)	Ag1–F1–Ag1^{i}	87.00(6)
N2^{ii}–Ag1–N3^{iii}	118.2(2)		

Symmetry codes: (i) x, ½ – y, 3/2 – z; (ii) ½ – x, ½ – y, z; (iii) ½ –x, y, 3/2 – z.

Table S3: Selected bond distances (Å) and angles (°) for $[Ag_4F(\mathbf{3})_2](OTf)_3 \cdot 3H_2O$.

Distance (Å)			
Ag1–F1	2.351(3)	Ag2–N3	2.249(5)
Ag2–F1	2.413(3)	Ag2–N4^{i}	2.314(5)
Ag1–N1	2.375(5)	Ag2–N5^{i}	2.491(5)
Ag1–N2	2.525(5)	Ag1···Ag1^{i}	3.1171(9)
Ag1–N6^{i}	2.242(4)	Ag2···Ag2^{i}	3.2036(9)
Angle (°)			
F1–Ag1–N1	107.00(12)	N3–Ag2–N4^{i}	129.63(19)
F1–Ag1–N2	103.74(12)	N3–Ag2–N5^{i}	109.76(17)
N1–Ag1–N2	87.97(15)	N4^{i}–Ag2–F1	107.82(13)
N6^{i}–Ag1–F1	121.23(12)	N4^{i}–Ag2–N5^{i}	81.81(17)
N6^{i}–Ag1–N1	122.25(17)	Ag1–F1–Ag1^{i}	83.05(14)
N6^{i}–Ag1–N2	107.72(15)	Ag1–F1–Ag2^{i}	175.443(16)
F1–Ag2–N5^{i}	110.38(14)	Ag1–F1–Ag2	97.068(17)
N3–Ag2–F1	112.60(12)	Ag2^{i}–F1–Ag2	83.18(14)

Symmetry code: (i) *y*, *x*, 1 − *z*.

Table S4: Selected bond distances (Å) and angles (°) for $[Ag_5F(\mathbf{2})_2](OTf)_4 \cdot 2H_2O \cdot C_3H_6O \cdot C_6H_6$.

Distance (Å)			
Ag1–F1	2.463(6)	Ag4–F1	2.397(7)
Ag1–N1	2.263(9)	Ag4–N4	2.248(11)
Ag1–N7	2.254(9)	Ag4–N11	2.223(10)
Ag2–F1	2.575(7)	Ag5–N5	2.436(11)
Ag2–N2	2.201(9)	Ag5–N6	2.294(11)
Ag2–N8	2.294(10)	Ag5–N12	2.215(10)
Ag2–N9	2.492(11)	Ag1···Ag2	2.9388(14)
Ag3–F1	2.500(6)	Ag1···Ag5	3.0845(16)
Ag3–N3	2.235(10)	Ag2···Ag3	2.9589(19)
Ag3–N9	2.498(11)	Ag3···Ag4	2.9735(16)
Ag3–N10	2.306(11)	Ag4···Ag5	2.9433(15)
Angle (°)			
N1–Ag1–F1	110.0(3)	N10–Ag3–N9	86.2(4)
N7–Ag1–F1	117.5(3)	N4–Ag4–F1	113.7(3)
N7–Ag1–N1	131.1(4)	N11–Ag4–F1	121.0(3)
N2–Ag2–F1	119.0(3)	N11–Ag4–N4	123.8(4)
N2–Ag2–N8	133.3(4)	N6–Ag5–N5	90.3(4)
N2–Ag2–N9	115.5(4)	N12–Ag5–N5	123.8(4)
N8–Ag2–F1	100.0(3)	N12–Ag5–N6	128.0(4)
N8–Ag2–N9	86.4(4)	Ag1–F1–Ag2	71.34(18)
N9–Ag2–F1	91.0(3)	Ag1–F1–Ag3	142.6(3)
N3–Ag3–F1	120.6(3)	Ag3–F1–Ag2	71.32(18)
N3–Ag3–N9	114.5(4)	Ag4–F1–Ag1	142.6(3)
N3–Ag3–N10	124.1(4)	Ag4–F1–Ag2	146.0(3)
N9–Ag3–F1	92.6(3)	Ag4–F1–Ag3	74.75(18)
N10–Ag3–F1	108.6(3)		

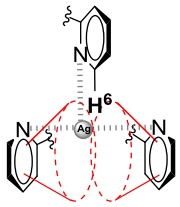

Figure S45: Schematic presentation of the shielding cones of the pyridine rings.

References

[1] Drev, M.; Grošelj, U.; Ledinek, B.; Perdih, F.; Svete, J.; Štefane B.; Požgan F. *Org. Lett*. **2018**, *20* (17), 5268–5273.

[2] Farley, S. J.; Rochester, D. L.; Thompson, A. L.; Howard, J. A. K.; Williams, J. A. G. *Inorg. Chem.* **2005**, *44* (26), 9690–9703.

[3] *CrysAlisPro*, version 1.171.38.46; Rigaku Oxford Diffraction: Yarnton, UK, 2018.

[4] Sheldrick, G. M. *Acta Cryst.* **2015**, *A71*, 3–8.

[5] Sheldrick, G. M. *Acta Cryst.* **2015**, *C71*, 3–8.

[6] Dolomanov, O. V.; Bourhis, L. J.; Gildea, R. J.; Howard J. A. K.; Puschmann H. *J. Appl. Crystallogr.* **2009**, *42*, 339–341.